STRAIN AND GRAIN SIZE ANALYSIS OF A DEFORMED ARCHEAN SUBAQUEOUS PYROCLASTIC FLOW

STRAIN AND GRAIN SIZE ANALYSIS OF A DEFORMED ARCHEAN PYROCLASTIC FLOW, TEMAGAMI, ONTARIO

by

DAVID H. FROST

A Thesis

Submitted to the Faculty of Science

in Partial Fulfilment of the Requirements

for the Degree

Bachelor of Science

McMaster University

April, 1985

BACHELOR OF SCIENCE (1985)
(Geology)

McMASTER UNIVERSITY,
Hamilton, Ontario

TITLE: Strain and Grain Size Analysis of a Deformed Archean Pyroclastic Flow, Temagami, Ontario

AUTHOR: David Harold Frost

SUPERVISOR: Dr. P. M. Clifford

NUMBER OF PAGES: x , 66

Abstract

The Archean pyroclastic conglomerate studied has six clast types which can be condensed to four clast families based on lithology. The quartz clasts have an average strain of X:Y:Z=1.21:1:0.55 while the pumice clasts have an average strain of X:Y:Z=1.27:1:0.47. The difference is strain between these clast families can be attributed to their different viscosities. The quartz clasts have an assumed viscosity ratio between the clasts and the matrix of unity and are taken to represent the strain in the rock as a whole. The sulphide and black clasts have strain ratios much higher than the quartz because of recrystallization of the sulphide and cleavage formation effecting the black clasts.

The sedimentary structure of the deposit and its position between mafic pillow basalts indicate that the deposit is a result of the deposition of a subaqueous pyroclastic debris flow in a proximal environment.

ACKNOWLEDGEMENTS

I would like to express my thanks to Dr. P. M. Clifford for supervising this thesis and taking time to come to Temagami and chose this outcrop to study. I would also like to thank Andy Fyon for hiring me as an assistant in the mapping of the Temagami area and introducing the outcrop under study to Dr. Clifford. I would like to thank Len Zwicker for making thin sections and helping me slab my extremely large samples. Thanks must go to Jack Whorwood for his photography. A final thank you goes to Monica Niedermeyer, Brenda Hewitt and Don Evans for their help in typing the thesis.

TABLE OF CONTENTS

LIST OF FIGURES

LIST OF TABLES

LIST OF PLATES

CHAPTER ONE

INTRODUCTION

In a deformed conglomerate it is possible to establish the presence or absence of an original sedimentary fabric in the clasts. Grain size variations and sorting of the deposit can be characterized. Combining these features with the field associations of the deformed conglomerate should give some idea of the possible mode of emplacement of the conglomerate. In a deformed polymictic conglomerate a comparison of deformational behaviours (strain) of the different clast lithologies can be made.

The method of strain analysis also serves as a basis for identifying the presense of original fabrics. The determination of finite strain of a conglomerate can be made using the deformed shape of the clasts in the deposit. The final shape and orientation of the clasts are controlled by:

1)Initial clast shape and orientation

2)Viscosity or ductility contrast between the clast and the matrix

3)Shape and orientation of the strain ellipse.

Ramsay (1967) first outlined a method for strain determination assuming no ductility contrast between clasts and matrix and homogeneous strain. This method is still useful but its shortcomings have been discussed by a number of people. For example, Gay (1968) discussed the importance of viscosity contrasts between clasts and matrix when determining strain. Gay showed that with increasing viscosity ratio between the clast and matrix, the finite strain required to cause a change in the particle shape increased significantly. Evans et. al. (1980) have related the importance of clast size to the competence variations between clasts. They suggest that the clast size variation has more of an effect upon strain than the compositional variations. Dunnett (1969) and Dunnett and Siddans (1971) mention that it is possible to determine the presence of original fabrics in a deformed conglomerate. This was done by using the presence of asymmetries in a Ramsay type Rf vs ϕ scatter diagram.

The purpose of this study is two fold. Firstly a Dunnett (1969) type fabric study along with a grain size analysis will be done in an attempt to characterize the mode of emplacement of the conglomerate. Secondly, a strain analysis will be carried out in attempt to relate the differences in strain of the clast families to their lithology (or viscosity ratios).

The strain determined for the quartz clasts is assumed to be the strain for the entire unit. The validity of this assumption is based upon the fact that the majority of the clasts and almost all of the matrix are composed of the quartz. This would make the viscosity ratio of the quartz clasts approach unity and the strain on the quartz clasts to be homogeneous.

CHAPTER TWO

LOCATION AND GENERAL GEOLOGY

2.1 Location

Temagami is located in northwestern Ontario, approximately 800 km north of Toronto along Hwy 11. The study area is located in Strathy Township, immediately north of Temagami. Sampling was made on an outcrop located 1.6 km west of Hwy 11 on the south side of the Milne-Sherman road (Figure 2.1).

Figure 2.1 Location Map

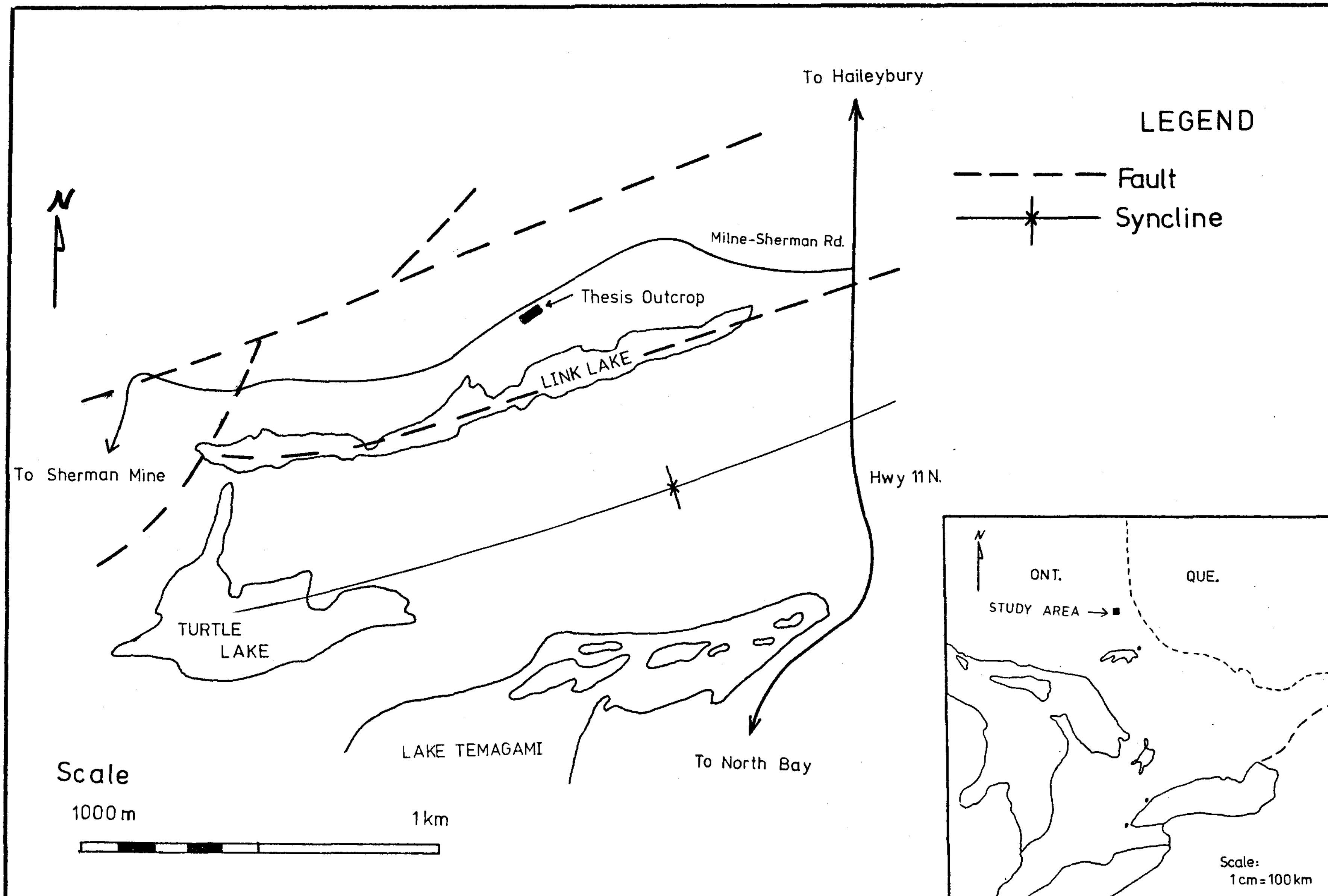
LEGEND
Fault
Syncline
N
To Haileybury
Milne-Sherman Rd.
Thesis Outcrop
LINK LAKE
To Sherman Mine
Hwy 11 N.
TURTLE
LAKE
LAKE TEMAGAMI
To North Bay
Scale
1000 m
1 km
N
ONT.
QUE.
STUDY AREA
Scale:
1 cm = 100 km

2.2 General Geology

2.2.1 Setting

The regional geology of the area consists of meta- sedimentary and meta-volcanic rocks forming a typical Archean greenstone belt. The area is metamorphosed to lower greenschist facies.

2.2.2 Previous Mapping

The Temagami area was mapped in the early 1900's by serveral geologists and more extensive regional mapping was done by Moorehouse (1942), Bennett (1978) and most recently Fyon in 1984/85.

2.2.3 Stratigraphy

Bennett (1978) noted two cycles of volcanism in the area. The cycles are characterized by the progression from massive mafic flows to pillowed mafic flows with a cap of intermediate to felsic flows, pyroclastics and their associated sedimentary rocks each having different emplacement mechanisms. Intrusive rocks in the area include quartz porphyries , diorites, gabbros and anorthositic gabbros. There are three granite plutons at the borders of the belt and late stage Nippissing diabase dikes cut across the area. Between the two volcanic cycles there is a major Algoma type banded silicate-oxide facies iron formation.

2.2.4 Structural Aspects

The area is highly deformed with many ENE trending features such as fold axes, faults, shear zones and stratigraphic contacts. The major structural feature in the area is a large scale tightly folded syncline with a subvertical east-northeast trending axial surface. The fold axis is deformed by a granitic pluton. This makes it difficult to determine any type of plunge on the fold axis. From available maps, it appears that the fold axis is horizontal or plunges gently to the west.

There are three main orientations of faults and shear zones in the area. There are north, northwest and east to northeast trending systems. The northwest trending system is parallel to the Sudbury dike swarm while the east to northeast trending system is concordant with bedding. None of the faults in the area show evidence of large scale movement.

2.2.5 Outcrop Location with Respect to Major Structures

The outcrop location with respect to the major syncline and faults is shown in Figure 2.1. The outcrop lies in the north limb of the syncline and is confined between two major bedding concordent, shears (or faults).

The fold axis of the syncline is approximately 1200m south of the outcrop while the Link Lake fault and the other bedding concordant fault are located 400m south and 450m north of the outcrop respectively.

Lithologically speaking, the outcrop is situated within a dominiately felsic volcanic and pyroclastic horizon about 800m below the stratigraphic equivalent of the iron formation of the south limb.

2.3 Outcrop Description

The outcrop consists of interbedded mafic volcanics and felsic conglomerates. This can be seen in figure 2.3 (a). There is a penetrative cleavage through the outcrop oriented parallel to the local unit contacts (086°/88° S). There is a distinct lineation orientated vertically in the cleavage surface (or [XY] section).

The bedding contacts are oriented roughly at 86°/88° S and there is evidence of scouring of the conglomerate by the overlying mafic basalt (See Figure 2.3 b). The mafic volcanics are 5 meters thick on average. Pillows show the stratigraphic top to be to the south and also indicate a subaqueous environment of emplacement. These mafic volcanic are ankeritized. The felsic units are graded polymictic felsic conglomerates with an average thickness of 5 meters.

Figure 2.3(a) Outcrop of interbedded pillow basalt and felsic conglomerate

Figure 2.3(b) Scouring of the felsic unit by the overlying mafic basalt

(a)

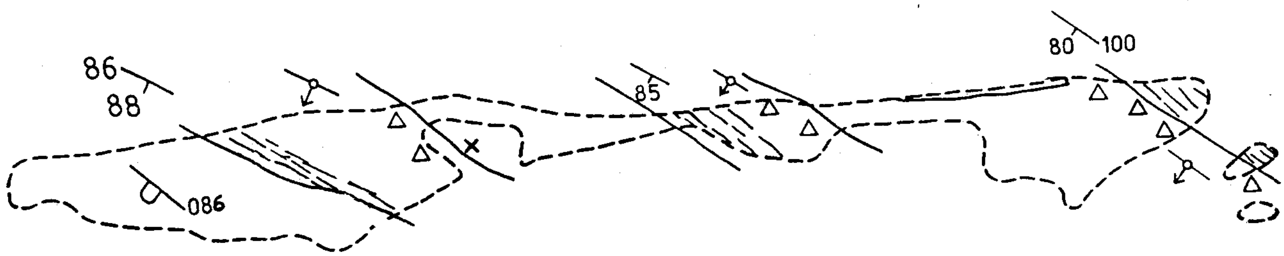

(b)

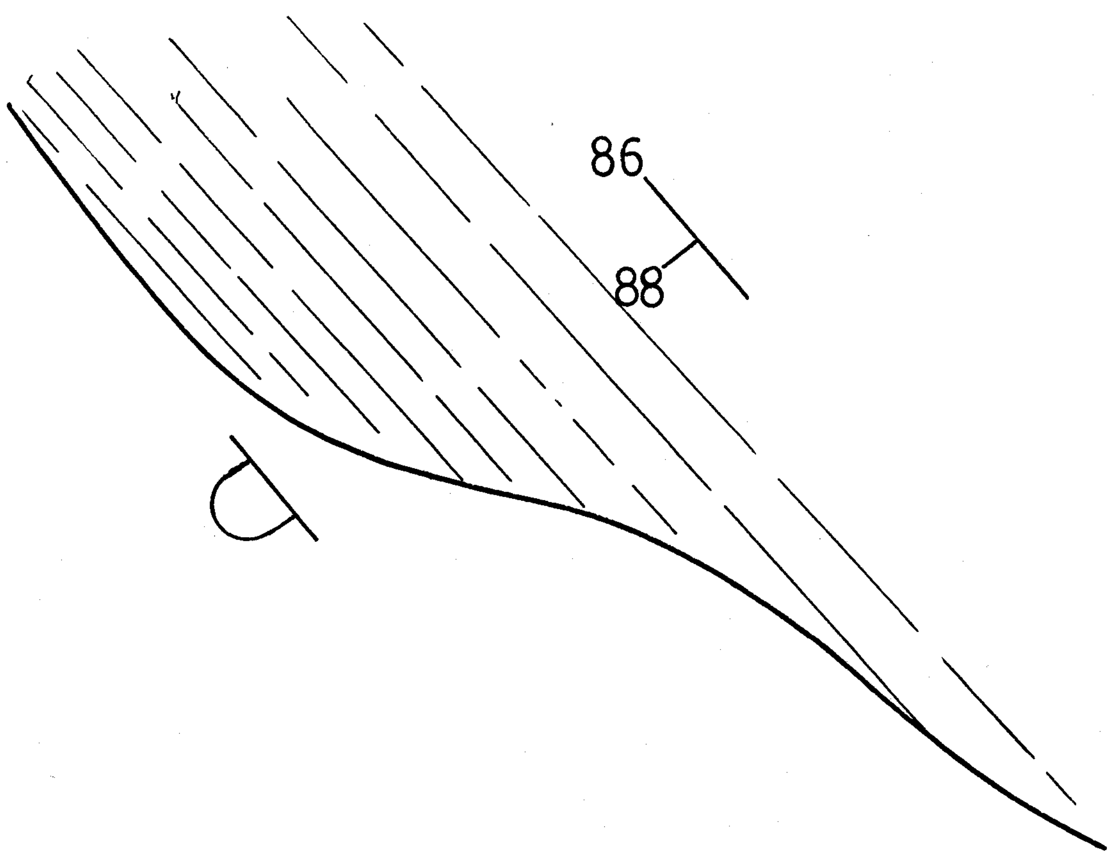

2.4 Felsic Conglomerate Description

2.4.1 General

The felsic unit studied is 5.3m thick. The unit grades from a base containing clasts as large as pebbles and cobbles to a fine laminated cherty top with grains less than 0.1mm in diameter (Plate 1). The clasts approximate ellipses in section with the long axis of the ellipse oriented roughly parallel to the cleavage and local unit contacts. There are relatively few clasts that have their long axis oriented at a high angle to the cleavage.

2.4.2 Clasts

There are six types of clasts within the unit.

1)Quartz, massive

2)Quartz, banded

3)Quartz, with quartz phenocrysts

4)Green, vesicular (Pumice)

5)Sulphide, pyrite

6)Black, wispy aggregates

These six clasts types are all recognized within the slabs. Typical examples and textures of each clast type is shown in Plates 2 and 3.

The <u>quartz rich clasts</u> are commonly elliptical in shape with well rounded margins and an aspect ratio about 2 to 1. There are also a few large blocky or angular quartz clasts occurring in the lower 2m of the unit, suggesting a short transport distance or a non-abrasion mode of transport of the clasts. The pumice clasts are characterized by their green color and the presence of vesicles. The pumice clasts are generally elliptical in shape and have aspect ratios of about 3 to 1. Plate 3(A) shows a pumice clast that has one end deformed by a small quartz clast. The black clasts occur as highly stretched out wisps or sheets with irregular ends, often with aspect ratio of up to 5 to 1. The sulphide clasts are recognized by the distinct iron-oxide strain on the outcrop. The shape of these clasts vary from round masses to stretched out and disseminated pyrite.

Thin sections of each clast type help to define the clast types. Three types of quartz rich clasts are composed largely of very fine grained (0.05mm) polycrystalline quartz with minor flakes of very fine grained (0.02mm) muscovite (Figure 2.4.3). Many of the massive quartz clasts have some carbonate alteration at their edges. The banding in some clasts is defined by the presence of bands of carbonate alteration in the clast. These probably represent zones of weakness within the clast. The quartz phenocrystic clasts have anhedral quartz phenocrysts of about 0.1mm. The green clasts are highly altered to calcite and muscovite and commonly have inclusions of quartz and opaques. This alteration suggests an original composition quite different from that of the other clast families. The black wisps are composed of muscovite and chlorite. The boundaries of these clasts are sharp but the presence of lensoidal shaped polycrystalline quartz within these clasts makes their origin suspect. The opaques vary from anhedral masses to elongate masses of euhedral disseminated grains.

Plate 1

Grading in the felsic unit as shown by slabs from three positions within the unit.

A) Sample 2 (Top)

B) Sample 10

C) Sample 3 (Base)

Note the laminations in sample 2 from the fine grained top of the unit.

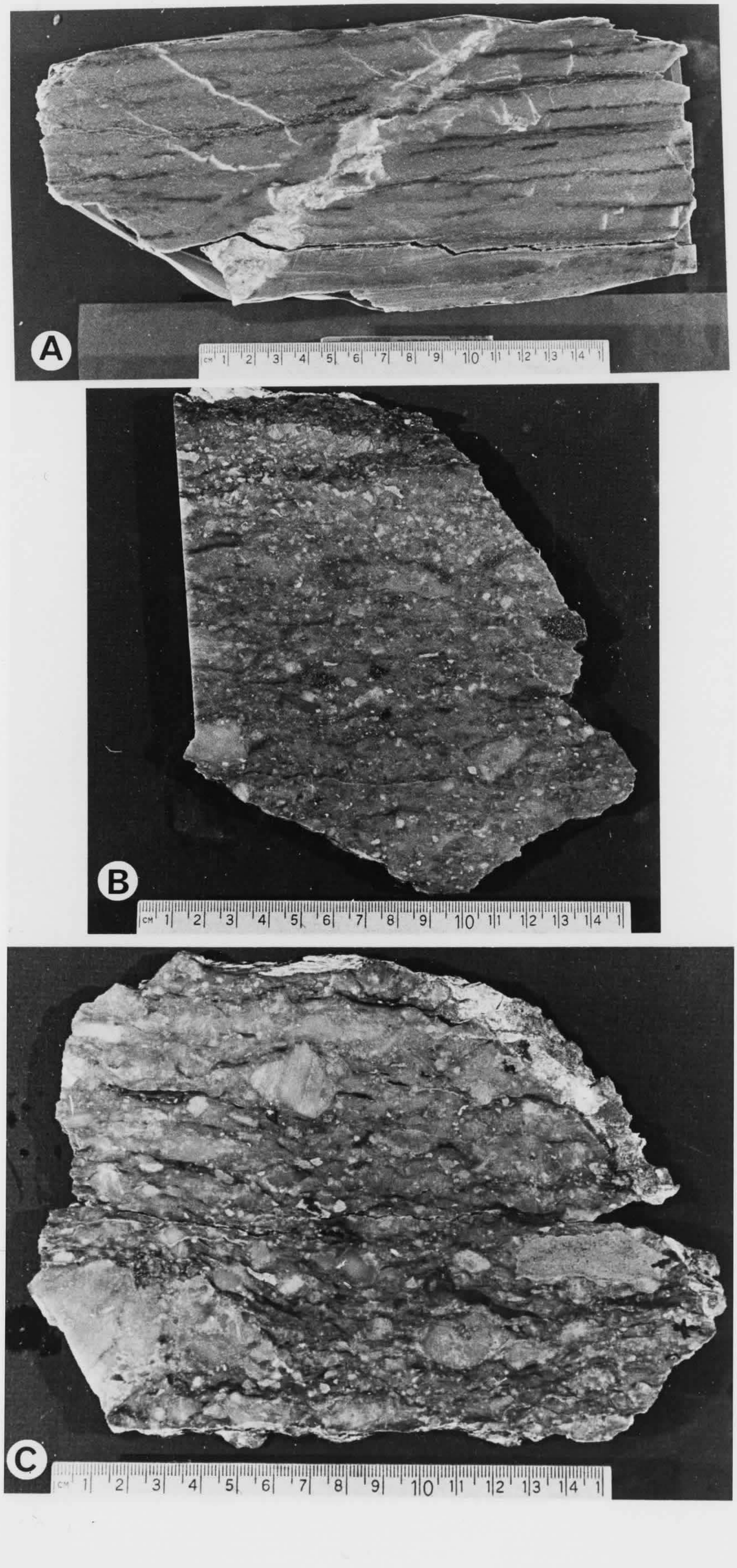
A
B
C

Plate 2

Clast types within the felsic unit. The width of the pictures are 4 cm.

A) Quartz, massive

B) Quartz, banded

C) Quartz with quartz phenocrysts

(continued on plate 3)

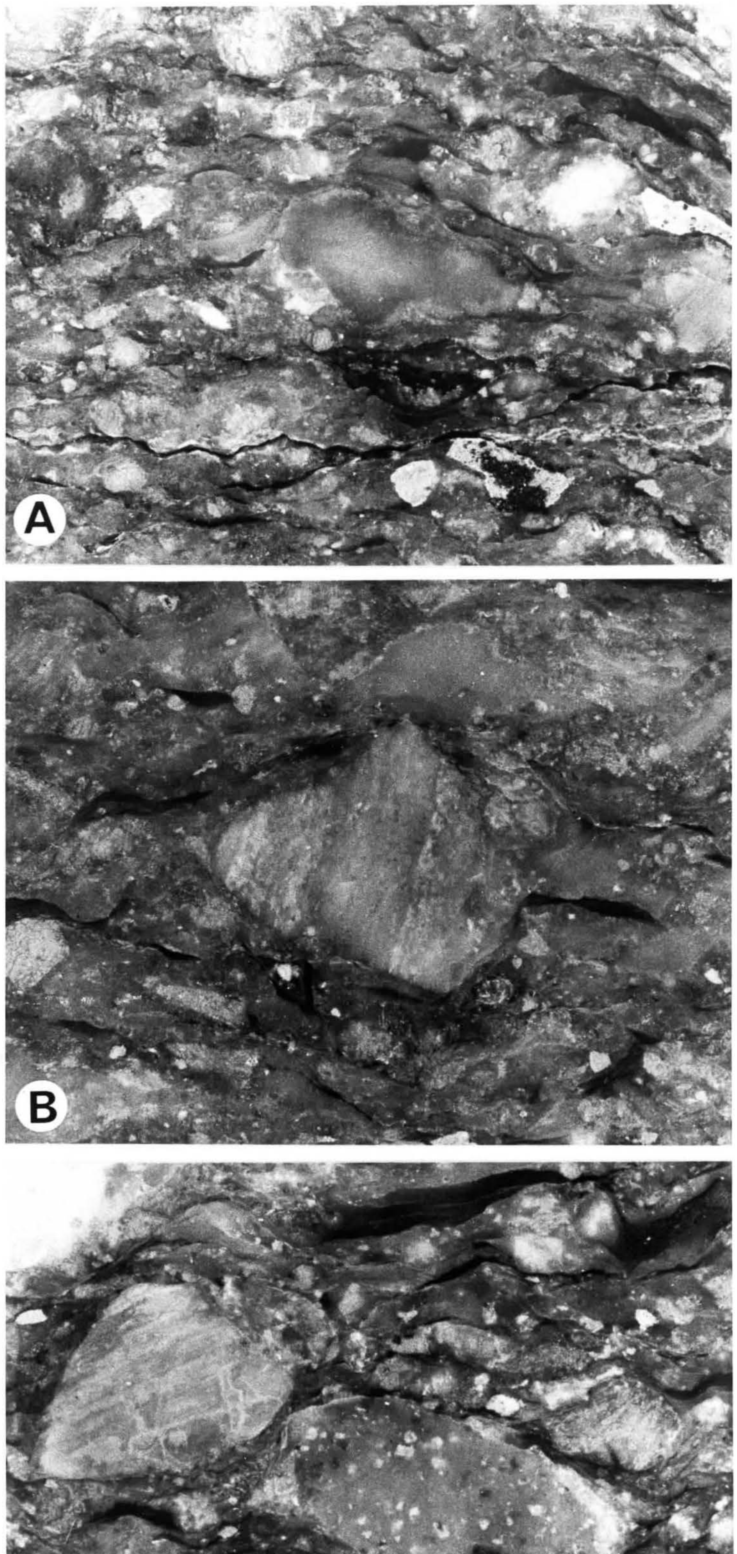
A
B
C

Plate 3

Clast types within the felsic unit (continued).

The width of the pictures are 4 cm.

A) Pumice, green vesicular

B) Sulphide, Pyrite

C) Black, wispy

Note the pumice and the black clasts being deformed by adjacent quartz clasts.

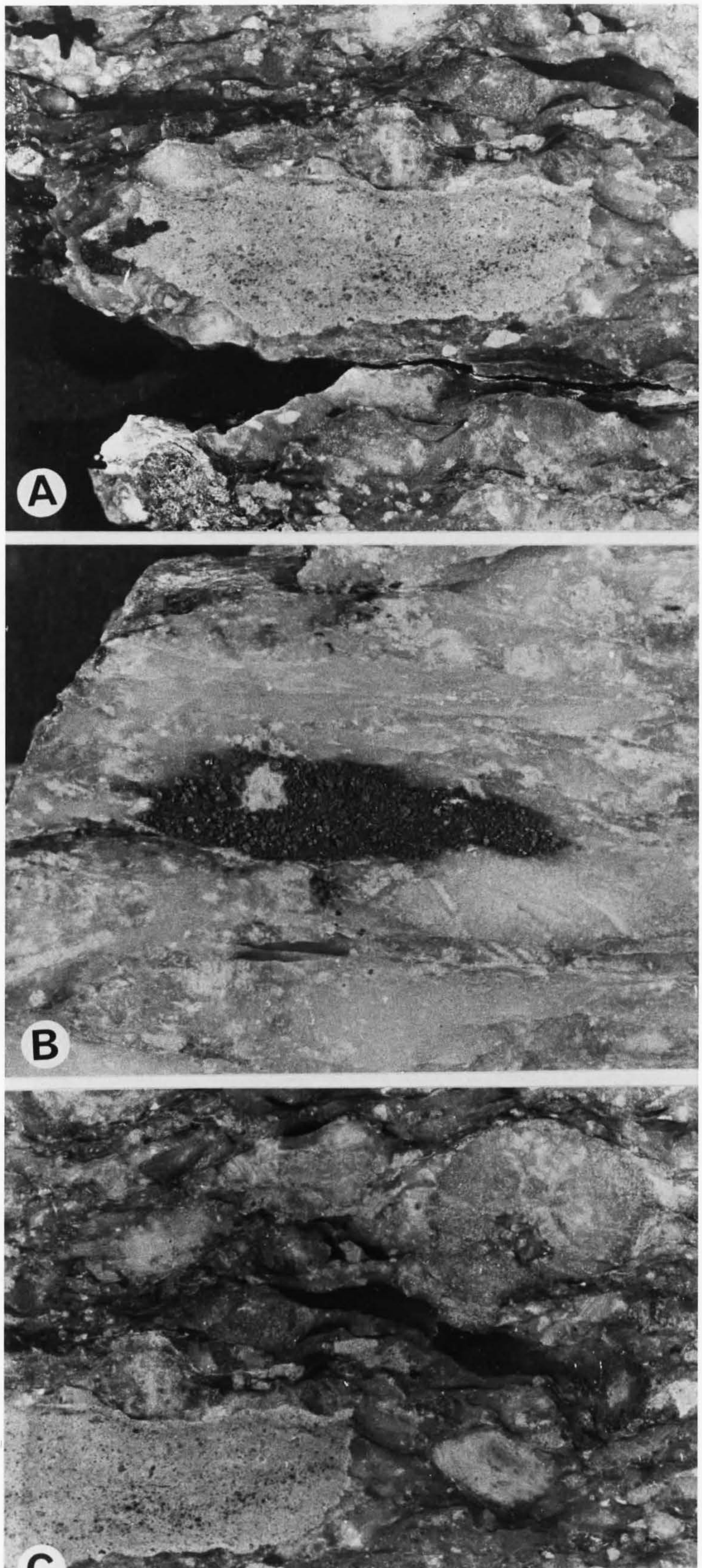
A
B
C

2.4.3 Relationship Between Clasts and Cleavage

All the clasts exhibit a definite preferential orientation of long axes roughly parallel to the cleavage (S_1). The cleavage generally anastomoses about the more equant quartz rich clasts and rarely transects these clasts. The banding in the banded quartz clasts shows no preferred orientation relative to either the cleavage or the long axis of the clast. This implies that the banding is an original feature in the clasts. The cleavage also flows around the green clasts but in many cases the cleavage cuts through the clast along the long axis. The sulphides and the black wisps are generally cut by the cleavage and are located in the cleavage planes. This could be a response of cleavage formation in areas of weaker and easily strained clasts or the forming of these clasts in the cleavage areas.

In the thin sections, the cleavage can be seen anastamosing about small clasts. The degree of anastomosis is quite different in the XZ orientation than in the YZ orientation (Figure 2.4.3). These differences are a reflection of the different strain ratios between the two orientations.

2.4.4 Laminations

The top 1.5 or 2.0 meters of the unit is characterized by the presence of laminations on the surface of the outcrop (Plate 1). The laminations appear to be the cleavage that is no longer anastomosing about clasts and is a planar feature. The laminations are oriented within the cleavage and parallel to the local unit contacts.

Figure 2.4.3

Photomicrographs and sketches of representative cleavages from Sample 5. The degree of anastomosis suggests the level of strain in the section.

a) XZ section

b) YZ section

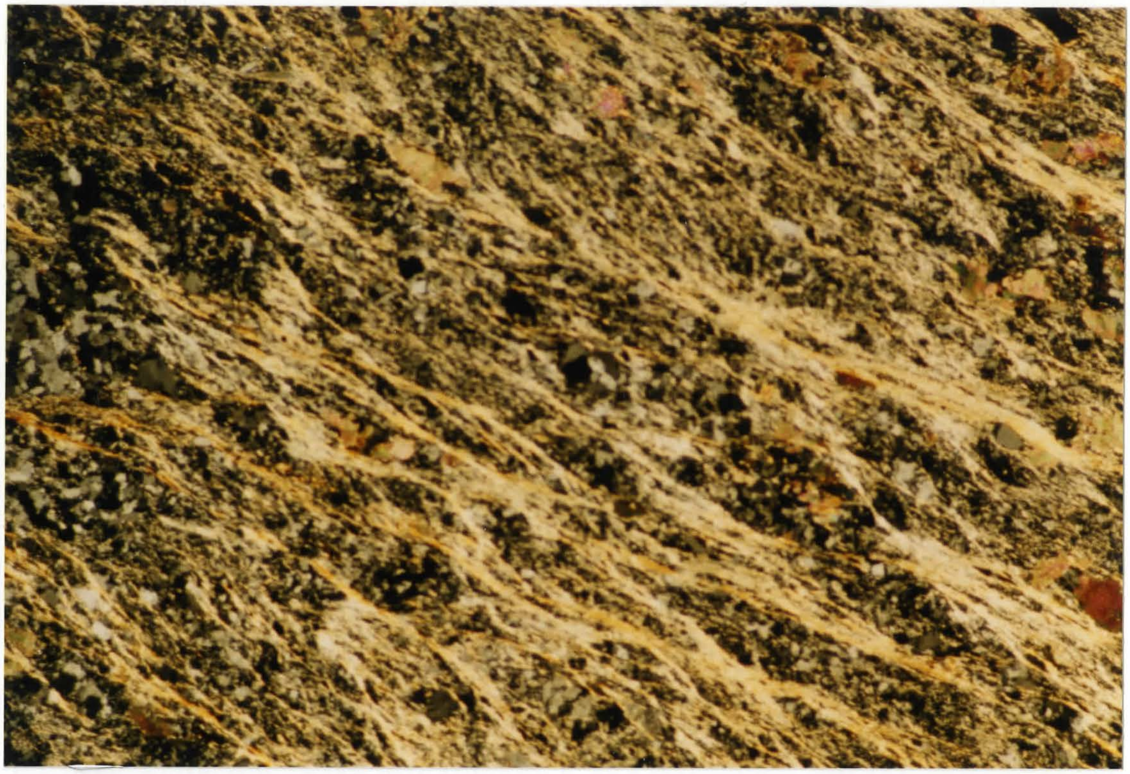

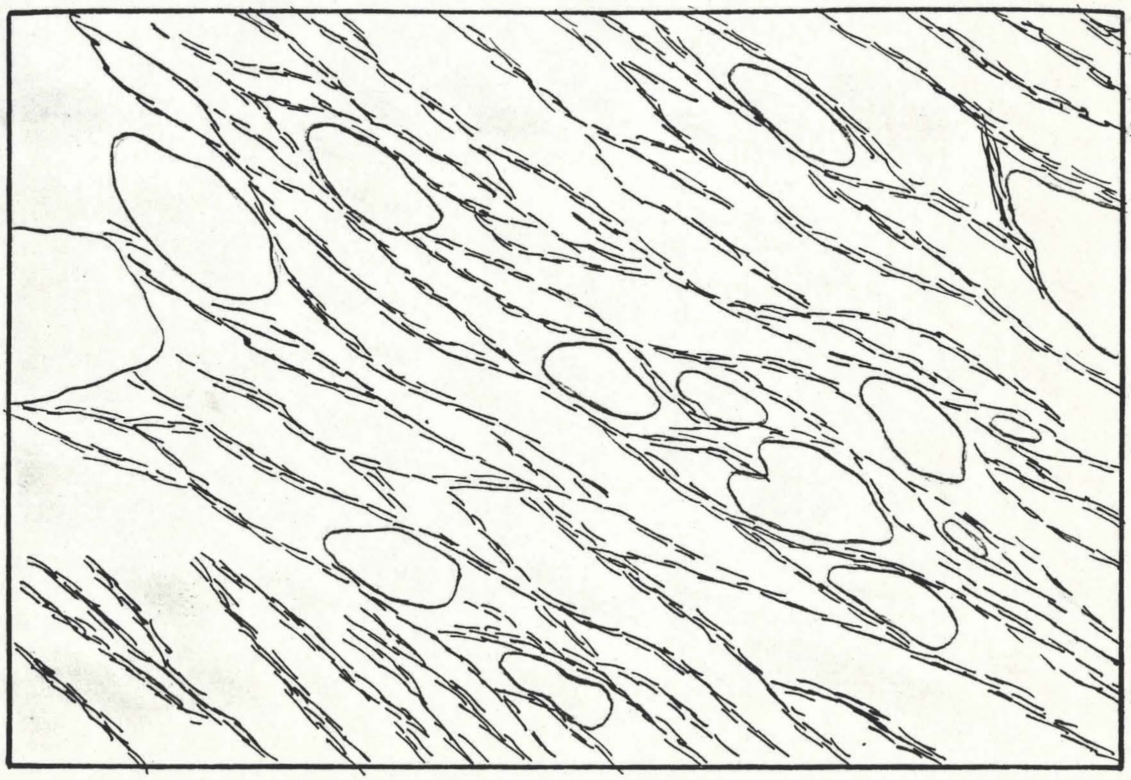

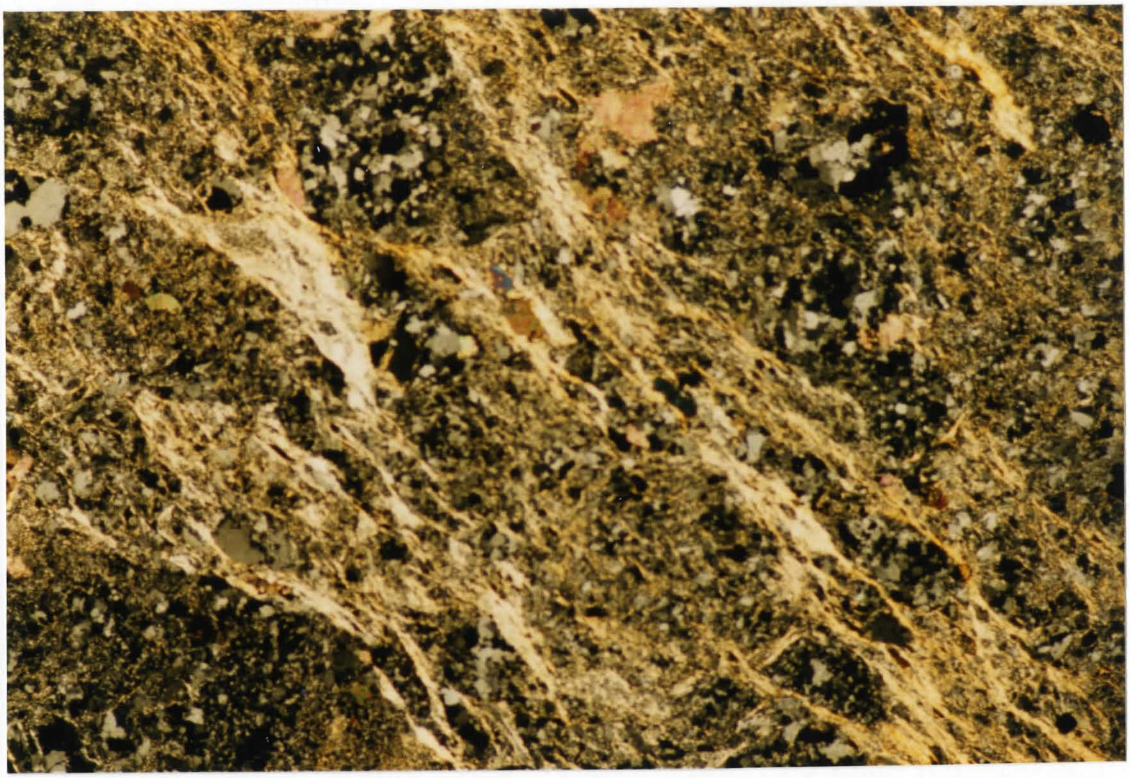

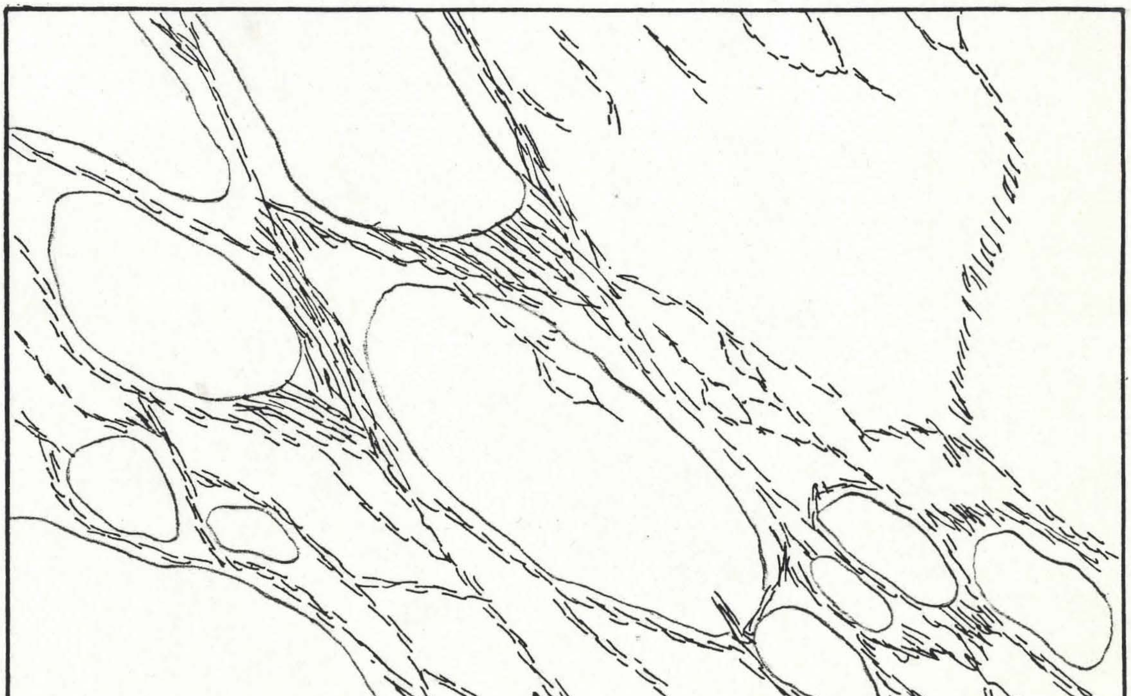

CHAPTER THREE

METHOD

The methods of determining the presence of an original fabric and comparing deformational behaviours between clasts of different lithologies both involve a Ramsay (1967) type strain analysis.

3.1 Sample Collection

In order to obtain strain data from the conglomerate, oriented samples were collected and taken back to the lab. The samples were very large in order to insure that a sufficient number of clasts of each family would be available for the calculation of reproducible strain values. Measurement of axial ratios of clasts was done on the macroscopic scale, therefore only the samples from the coarser base of the unit were used for the strain calculation. Sample locations can be seen in Figure 3.1 and the samples used for strain analysis are marked by an asterisk.

Figure 3.1

Sample Locations

Grain size and strain analysis was done on slabs from samples marked by an asterisk *. (4,3,1,10) Thin section measurements were from samples marked with a check . (13,5,6,2) Positions of field measurements of maximum clast size are shown by a dot on the outcrop.

SAMPLE LOCATIONS

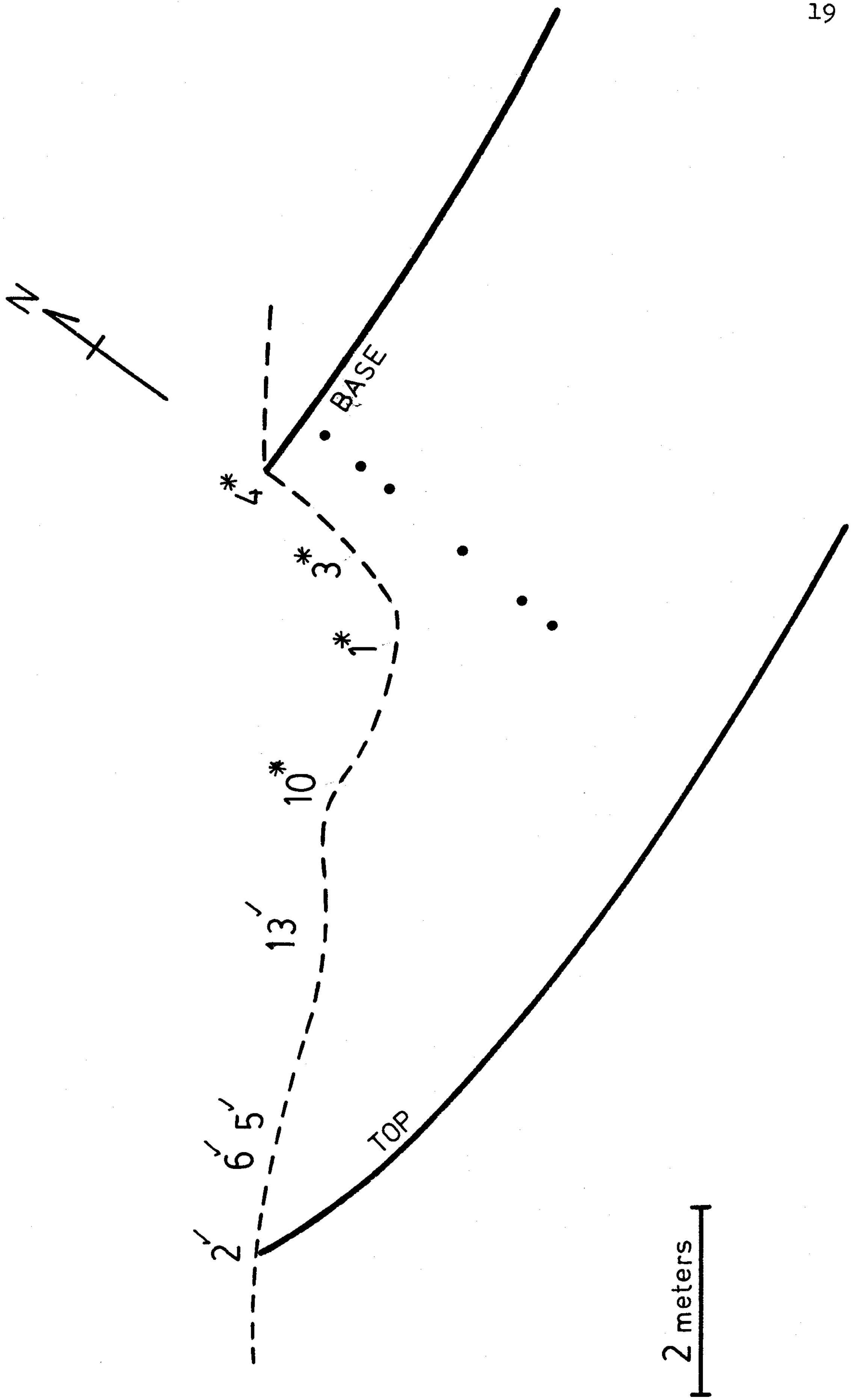

3.2 Slab Preparation

The presence of a penetrative cleavage limits the cutting to the production of two orthogonal slabs oriented perpendicular to the cleavage. The third mutually orthogonal face is not needed for the determination of three dimensional strain as noted by Ramsay (1967). Dunnett (1969) points out that the cleavage plane represents the XY principal plane of strain. The sections cut parallel to the lineation represent the XZ plane and the sections cut normal to the lineation represent the YZ plane. The precision of cutting in the lab is assumed to be $\pm$ 5°. The orientation of the XZ and YZ principle planes of strain are 086°/88°S and 086°/2°N respectively. Figure 3.2 shows a typical sample with the positions of the principle planes of strain assumed by the author. The orientation of the clasts, the cleavage plane and the lineations within the cleavage plane are also shown.

Figure 3.2

Typical sample sketch showing positions of the principle planes of strain, the cleavage, and the lineation on the cleavage plane.

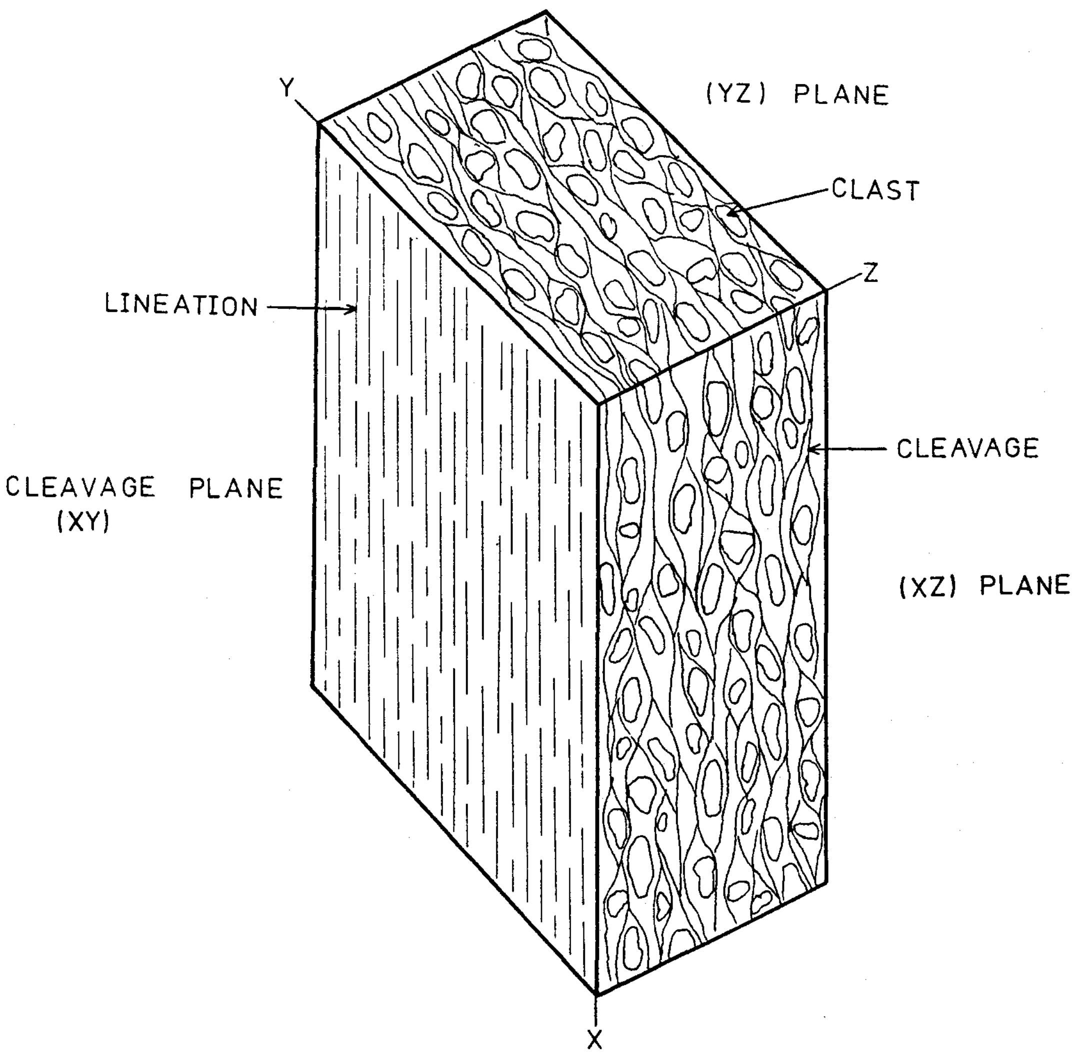
Y
(YZ) PLANE
CLAST
Z
LINEATION
CLEAVAGE
CLEAVAGE PLANE
(XY)
(XZ) PLANE
X

3.3 Data Collection

The clasts were divided into four families on the basis of composition. All data collected were recorded separately for each clast family. A reference axis was drawn at $45^\circ \pm 5^\circ$ to the cleavage across the front and back of each slab. It is important to note the apparent reversal in orientation of grains on the back of the slabs compared to the front.

3.3.1 Grain Shape and Orientation

For each clast, the long axis (2a or X), the short axis (2b or Y), and the angle from the reference line to the long axis (Ø) is recorded. To make the clasts more obvious to the naked eye, water and a sheet of mylar was placed over the slabs. Clasts were then traced onto the mylar sheets and measured directly off the mylar.

From the measured dimensions of the clasts, the axial ratios were calculated. The axial ratio for each clast was plotted against the orientation in a typical Ramsay scatter diagram. The result is a Rf vs Ø plot for each clast family, for each of the two orthogonal slabs from the samples. The tectonic strain (Rs) is approximated by calculating the logarithmic mean of the Rf values. The mean orientation of the clasts was calculated using a (Rf-1) weighted vector summation (Hsu 1971).

$$\bar{\varnothing} = \mathrm{Tan}^{-1}\left(\sum_{n=0}^{i} n_i \cos \varnothing \Big/ \sum_{n=0}^{i} n_i \sin \varnothing\right)$$

where; $\bar{\varnothing}$ = mean orientation

$\varnothing$ = long axis orientation

n_i = Rf - 1

Rf = axial ratio

The weighted vector method is used because clasts with a Rf = 1 should not have any weight on the calculation of mean orientation while clasts with a larger Rf value should have more weight put on the mean orientation calculation (Hsu,1971).

Using the calculated tectonic strain ratios, the axial ratios of the strain ellipsoid were calculated for each clast family at each sample location. The strain ellipsoids were then represented graphically on a deformation plot.

3.3.2 Clast Size

To determine clast diameters, the clast size measurements of long and short axes (X(orY) and Z) from the strain data were used. Therefore, all the grain size data comes from the coarser basal section of the unit. The samples used in the calculations can be seen in figure 3.1 and are marked by an asterisk.

The area of an ellipse with major and minor axes (X(orY) and Z) was calculated for each clast. From this, the nominal diameter (D) of a circle of equivalent area to the ellipse was calculated for each clast.

Graphs relating to frequency of occurence of each clast family was plotted against the clast nominal diameter. This was repeated for each sample. Cumulative abundance curves, using phi(0) sizes, were plotted for each clast family at each sample location.

Graphs relating the variation of mean grain diameter of each clast family with the position above the base of the unit were plotted using the data from the four samples. This type of plot was repeated using maximum clast size measurements made in the field. Finally, in order to determine a grain size variation in the fine grained top section of the unit, this type of plot was repeated using maximum grain (clast) sizes seen in the thin sections. The loccation of the maximum clast size measurements and the thin sections are shown in figure 3.1 .

CHAPTER FOUR

RESULTS

4.1 Strain Analysis

4.1.1 Rf vs. Ø Diagrams

The strain data are shown in Ramsay-type Rf vs. Ø diagrams. Diagrams for each clast family are plotted for the two orientations of slabs that were cut from the samples. The scatter diagrams in figures 4.1.1.1 to 4.1.1.4 represent four samples from the basal section of the unit. The shape of the Rf vs. Ø plot represents the degree of strain which a particular group of clasts has suffered in the measured section. The strain values for each clast family from the two slab orientations were calculated and are listed in table 1. The strain ratios of the strain ellipsoids are also listed in table 1.

The scatter diagrams were symmetrical about an axis coincident with the cleavage plane. The cleavage plane was therefore set at $Ø=0^\circ$ and all points with negative Ø values were reflected across the $Ø=0^\circ$ axis, to improve the clarity of the distribution.

The orientation of the strain ellipsoid and its principal axes of strain (X, Y and Z) is constant for each clast family at each sample location. The only exception to this is the apparent switch in the X and Z axes for the sulphide clasts in sample 4. This fact should be taken very lightly because the strain value derived for the sulphide clasts in the slab oriented normal to the lineation is from only three measurements. This is definitely far from being sufficient to determine a satisfactory strain value. This value is therefore marked by an asterisk in table 1.

It is important to note that the orientation of the XY principle plane of strain is parallel to the local bedding (086°/88° S). This implies that the strain was irrotational with respect to bedding, and during deformation there was no differential rotation of the local bedding and the long axis of the clasts. This prevents any interpretation of the original sedimentary fabric by using methods described by Dunnett and Siddans (1971).

By definition, the strain values in the XZ orientation are greater than or equal to the strain values in the YZ orientations. This also holds true for the maximum axial ratios measured in the two orientations. The maximum axial ratios for most of the clast families measured in the slabs cut parallel to the lineation (XZ principal plane) are larger than those measured in slabs cut normal to the lineation (YZ principal plane), for each sample. In the XZ and YZ sections, the average strain ratios increase from the quartz, to the pumice, to the sulphide, and finally are highest in the black clasts.

The fluctuation angles in the sections vary from values of less than 90° to values of 180°. The XZ sections which have the highest strain ratios and highest axial ratios have the smallest fluctuation angles. These angles are generally less than 90° and rarely reach 180°. The fluctuation angles in sections oriented in the YZ principal plane are larger than the XZ plane and vary from less than 90° to 180°, depending upon the clast family.

The quartz clasts generally have fluctuation angles of 180°, thus the tectonic strain ratio for the quartz clasts, is less than the initial axial ratio of the quartz clasts. The pumice clasts have fluctuation angles varying from less than 90° to 180°. The fluctuation angles are generally less than 180°. This implies that the tectonic strain ratio for the pumice clasts may be greater than the initial axial ratio of the pumice clasts. The fluctuation angles of the sulphide clasts and the black clasts are highly restricted and are always less than 90°. This implies that the tectonic strain ratio for the sulphide and black clasts is greater than the initial axial ratio of these clasts.

Neither the scatter diagrams nor the strain values in table 1 show any obvious variation in the strain from the base upwards through the unit.

Figure 4.1.1.1 a-h

R_f vs 0 diagrams for Sample 4.

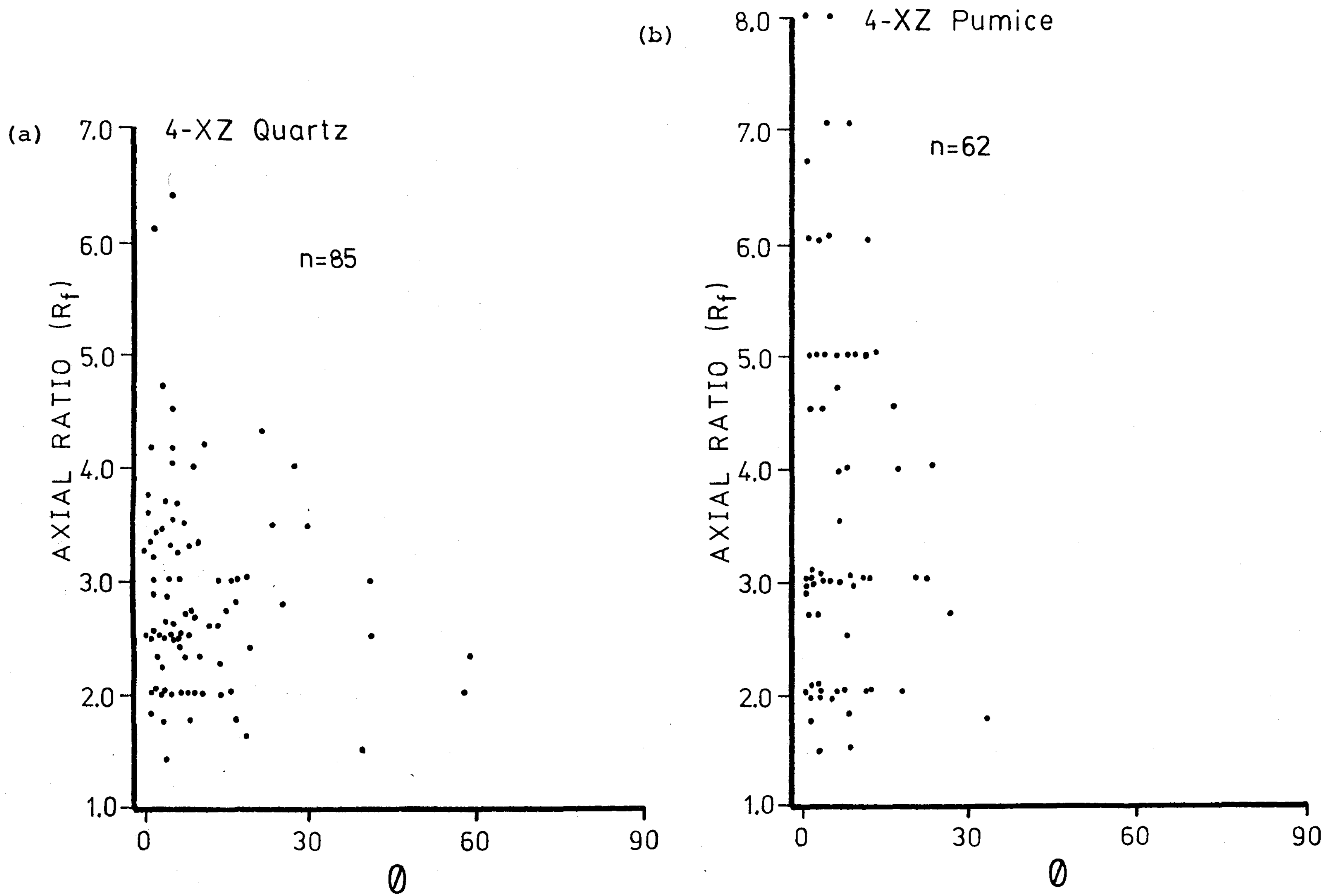
(a)
4-XZ Quartz
n=85
AXIAL RATIO (R_f)
7.0
6.0
5.0
4.0
3.0
2.0
1.0
0
30
60
90
Ø
(b)
4-XZ Pumice
n=62
AXIAL RATIO (R_f)
8.0
7.0
6.0
5.0
4.0
3.0
2.0
1.0
0
30
60
90
Ø

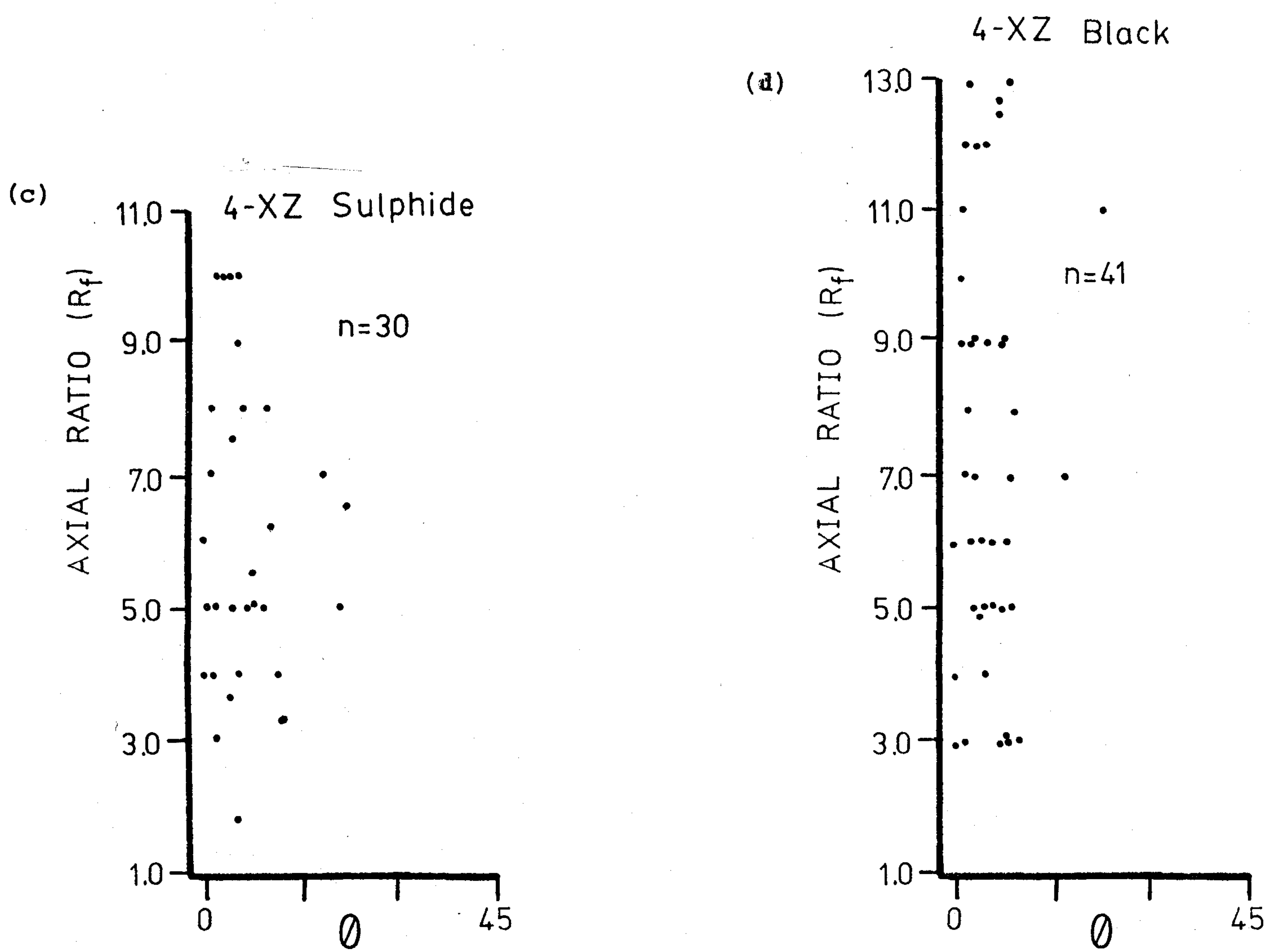
(c)
4-XZ Sulphide
n=30
AXIAL RATIO (R_f)
11.0
9.0
7.0
5.0
3.0
1.0
0
45
Ø
(d)
4-XZ Black
n=41
AXIAL RATIO (R_f)
13.0
11.0
9.0
7.0
5.0
3.0
1.0
0
45
Ø

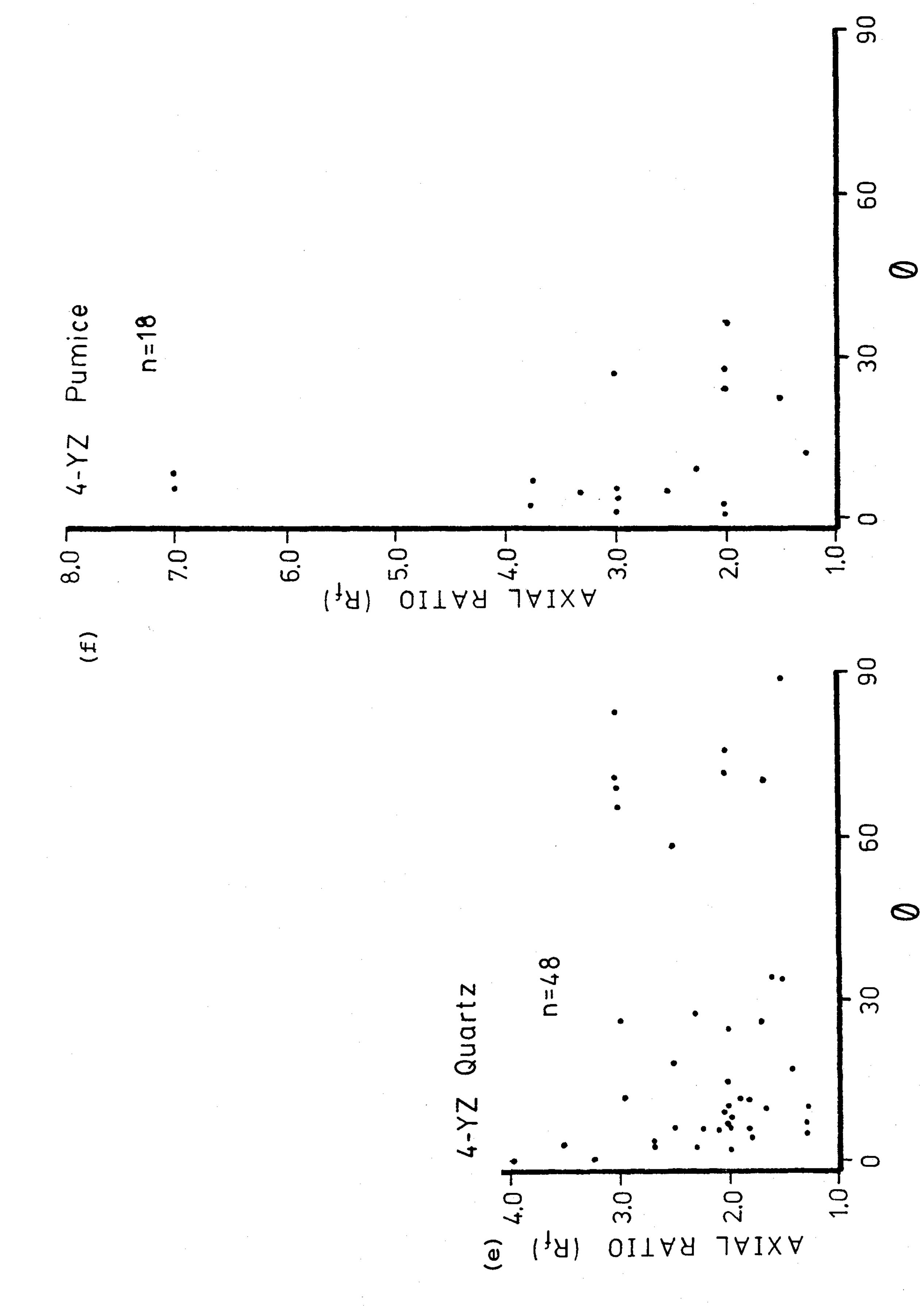
(f)
4-YZ Pumice
n=18
AXIAL RATIO (R_f)
8.0
7.0
6.0
5.0
4.0
3.0
2.0
1.0
0
30
60
90
Ø
(e)
4-YZ Quartz
n=48
AXIAL RATIO (R_f)
4.0
3.0
2.0
1.0
0
30
60
90
Ø

Figure 4.1.1.2 a-h

R_f vs 0 diagrams for Sample 3.

(g)

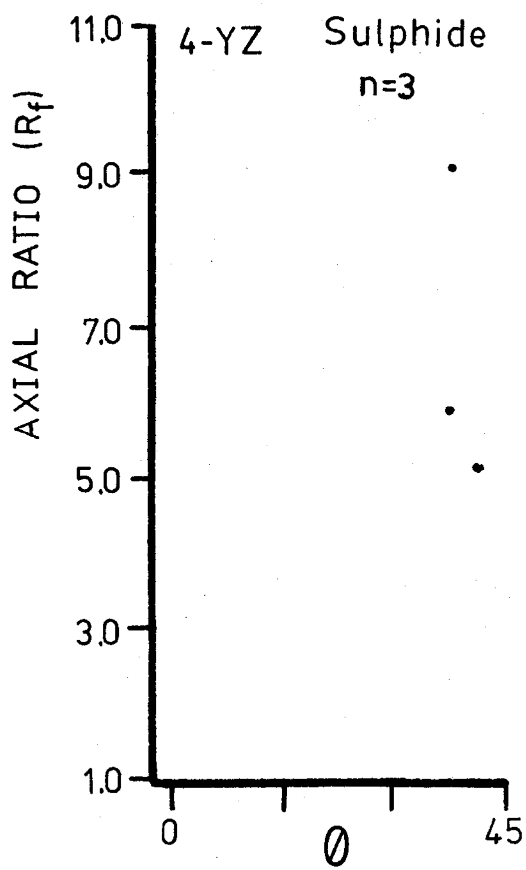
4-YZ Sulphide
n=3
AXIAL RATIO (R_f)
11.0
9.0
7.0
5.0
3.0
1.0
0
45
Ø

(h)

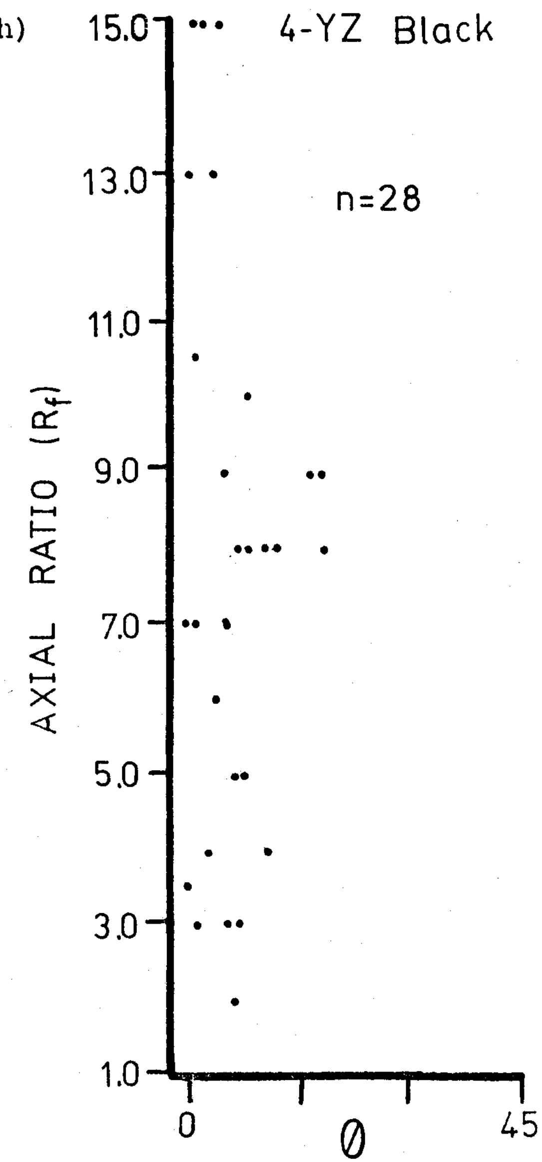
4-YZ Black
n=28
AXIAL RATIO (R_f)
15.0
13.0
11.0
9.0
7.0
5.0
3.0
1.0
0
45
Ø

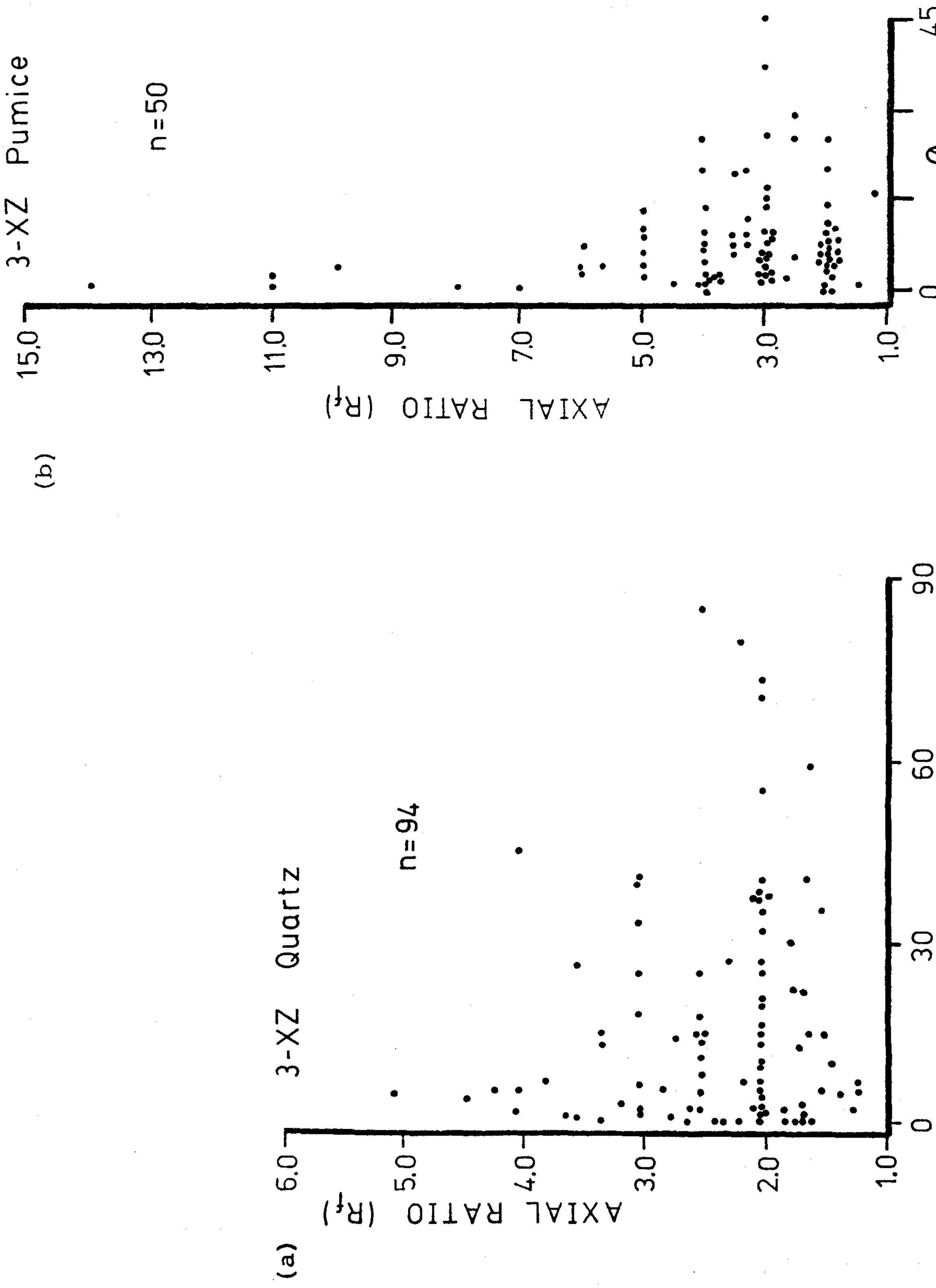

(a)
3-XZ Quartz
n=94
AXIAL RATIO (R_f)
6.0
5.0
4.0
3.0
2.0
1.0
0
30
60
90
Ø
(b)
3-XZ Pumice
n=50
AXIAL RATIO (R_f)
15.0
13.0
11.0
9.0
7.0
5.0
3.0
1.0
0
45
Ø

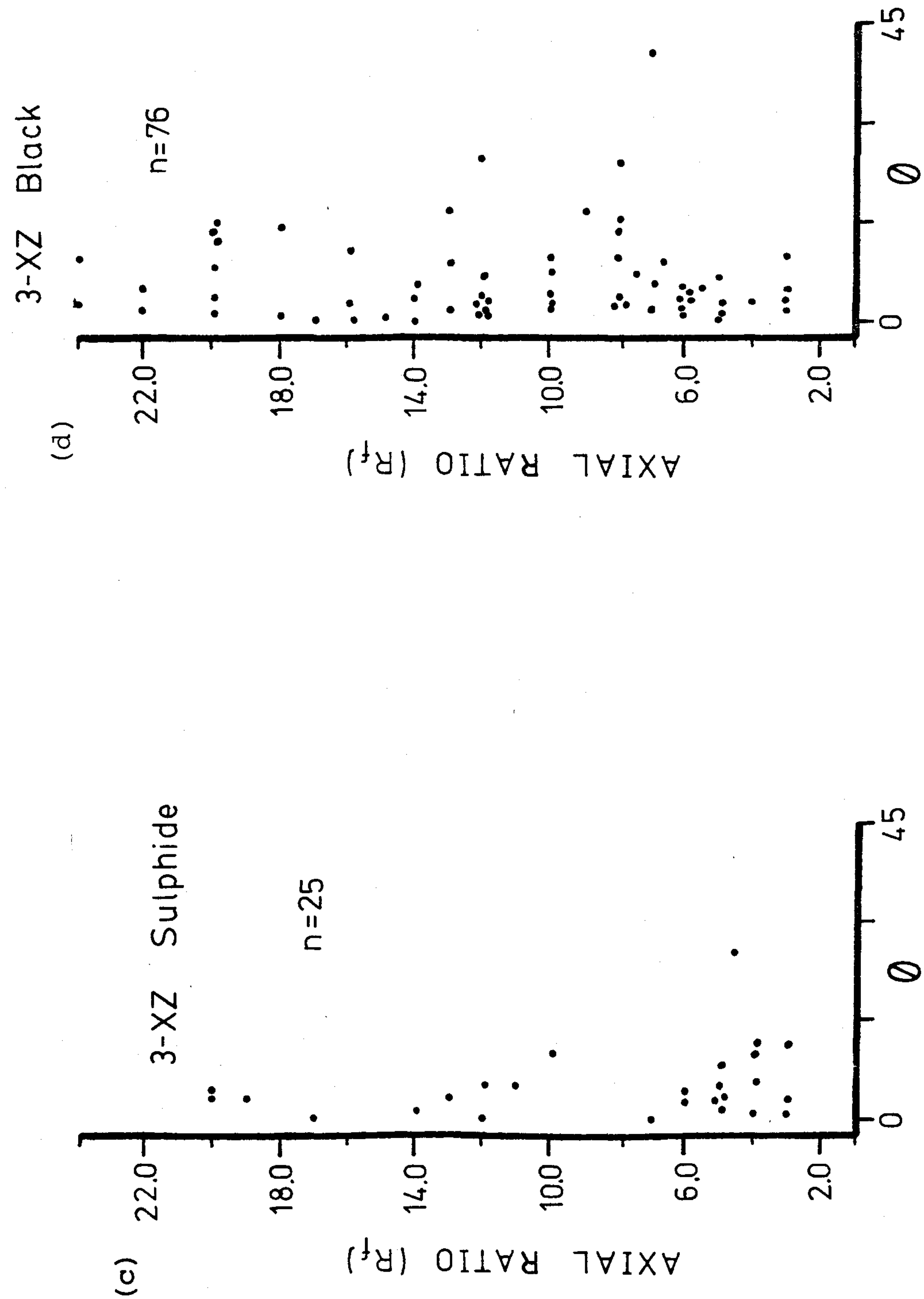
(d)
3-XZ Black
n=76
AXIAL RATIO (R_f)
22.0
18.0
14.0
10.0
6.0
2.0
0
Ø
45
(c)
3-XZ Sulphide
n=25
AXIAL RATIO (R_f)
22.0
18.0
14.0
10.0
6.0
2.0
0
Ø
45

(e)

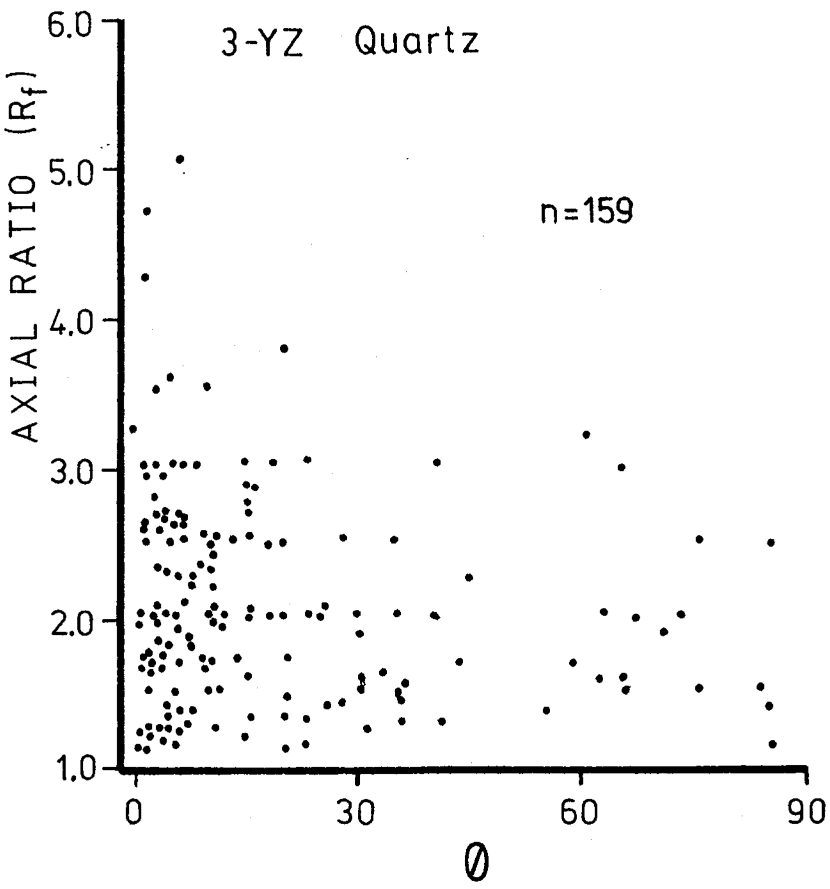
3-YZ Quartz
n=159
AXIAL RATIO (R_f)
6.0
5.0
4.0
3.0
2.0
1.0
0
30
60
90
Ø

(f)

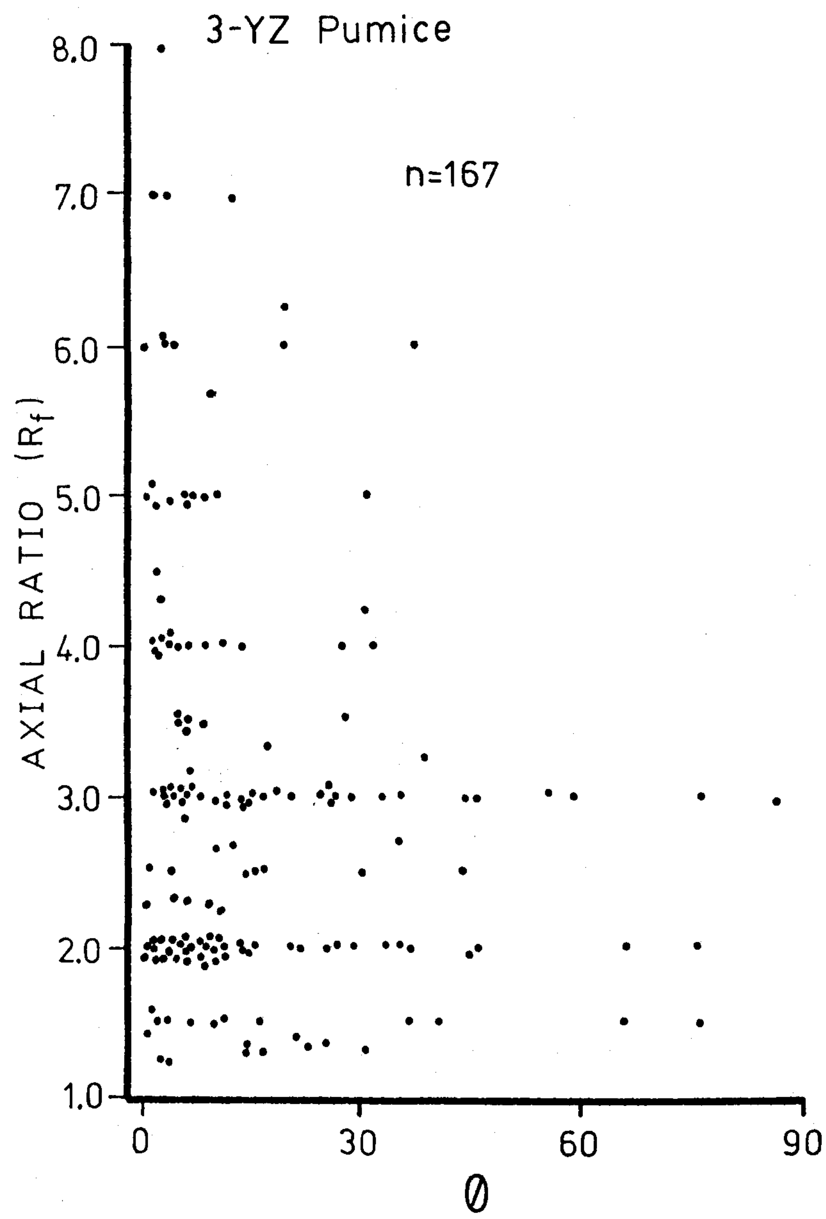
3-YZ Pumice
n=167
AXIAL RATIO (R_f)
8.0
7.0
6.0
5.0
4.0
3.0
2.0
1.0
0
30
60
90
Ø

(g)

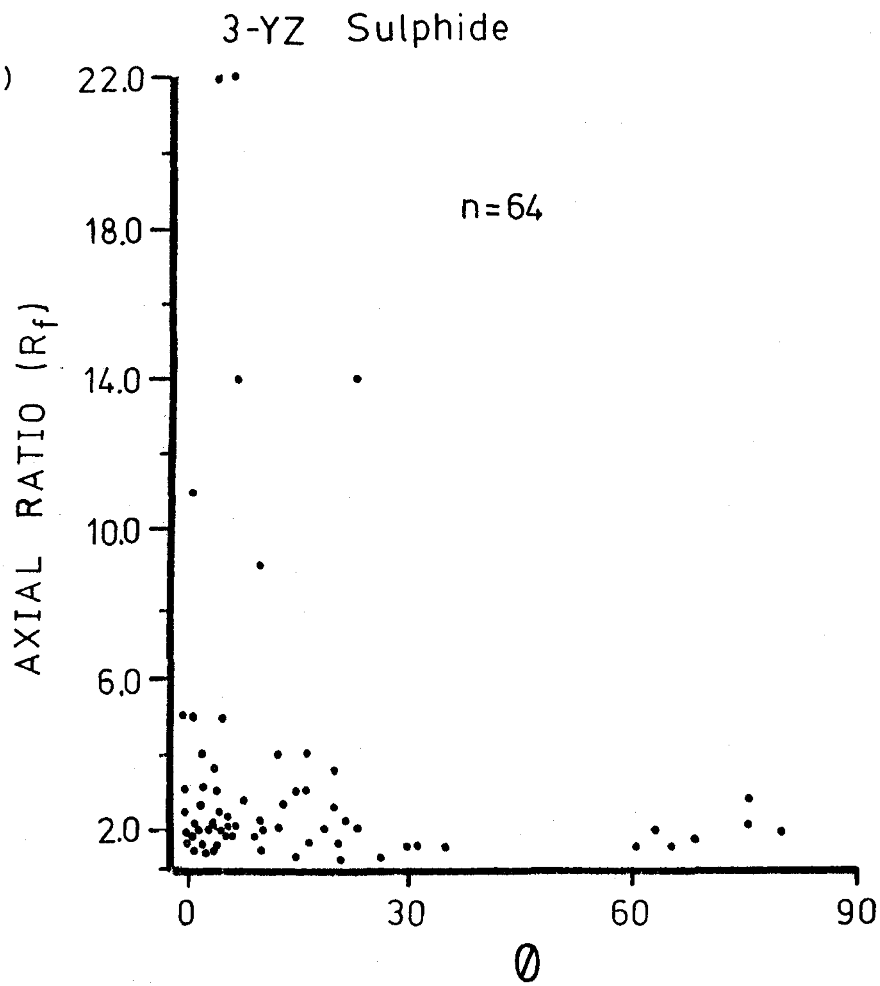
3-YZ Sulphide
n=64
AXIAL RATIO (R_f)
22.0
18.0
14.0
10.0
6.0
2.0
0
30
60
90
Ø

(h)

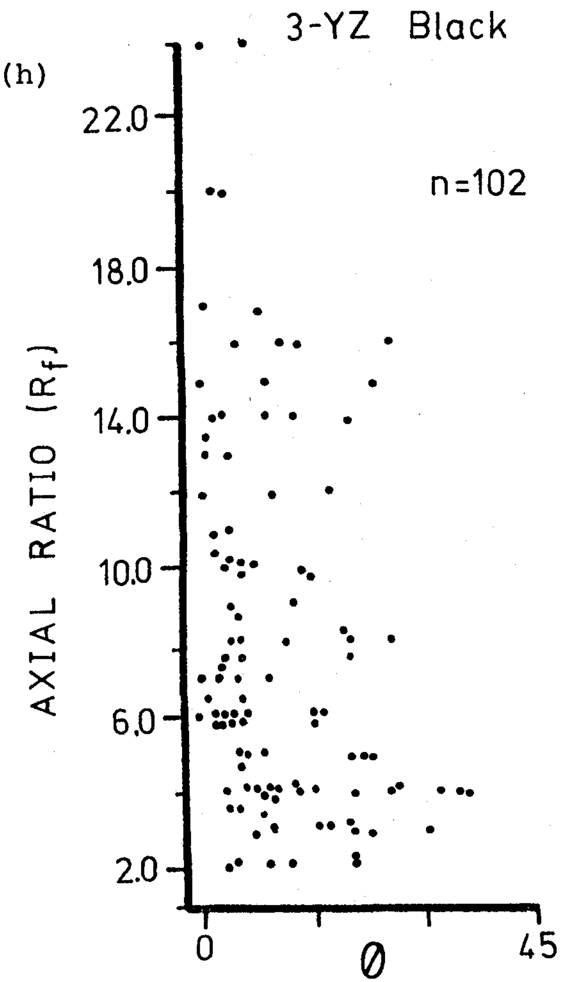
3-YZ Black
n=102
AXIAL RATIO (R_f)
22.0
18.0
14.0
10.0
6.0
2.0
0
45
Ø

Figure 4.1.1.3 a-h

R_f vs 0 diagrams for Sample 1.

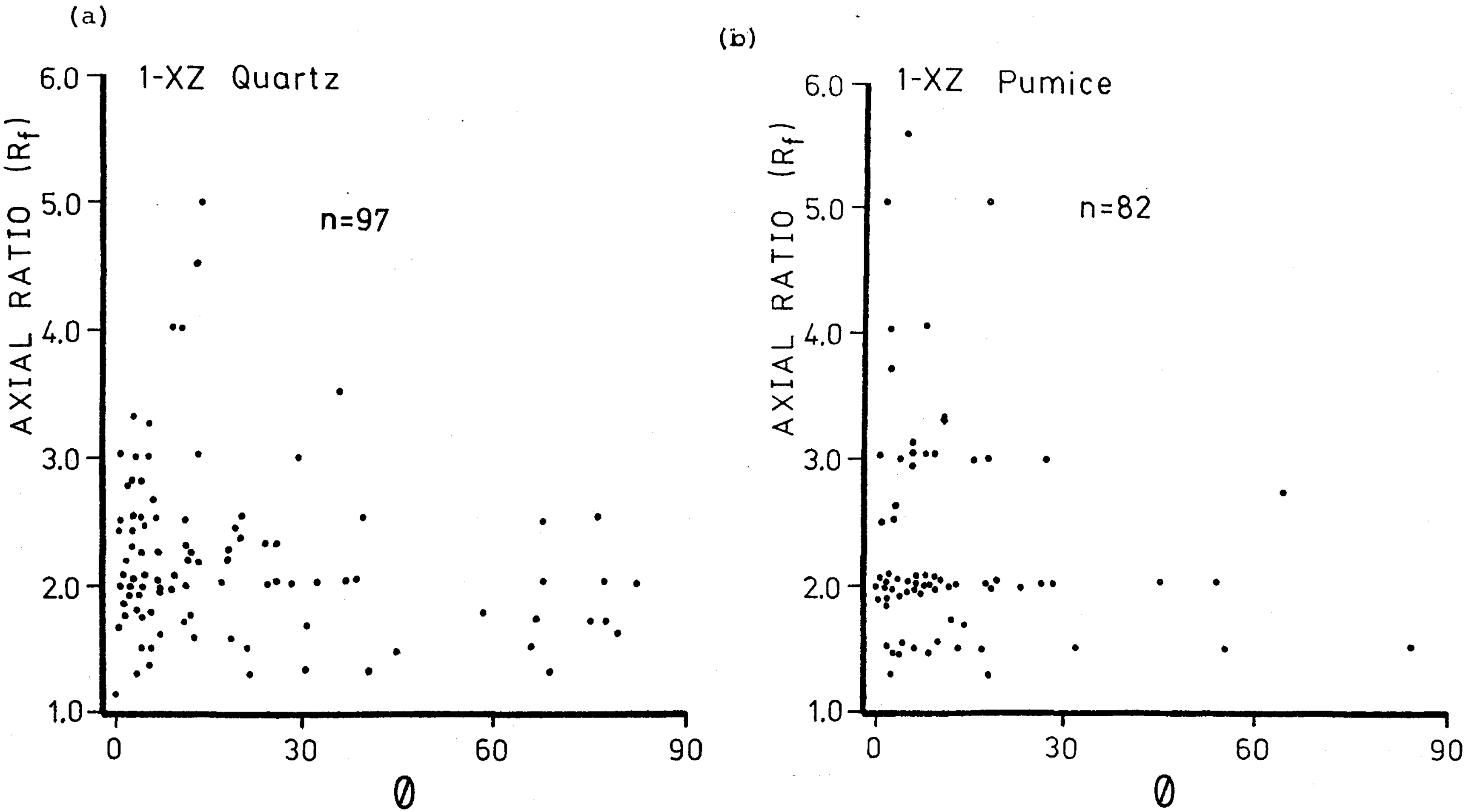
(a)
1-XZ Quartz
n=97
AXIAL RATIO (R_f)
6.0
5.0
4.0
3.0
2.0
1.0
0
30
60
90
Ø
(b)
1-XZ Pumice
n=82
AXIAL RATIO (R_f)
6.0
5.0
4.0
3.0
2.0
1.0
0
30
60
90
Ø

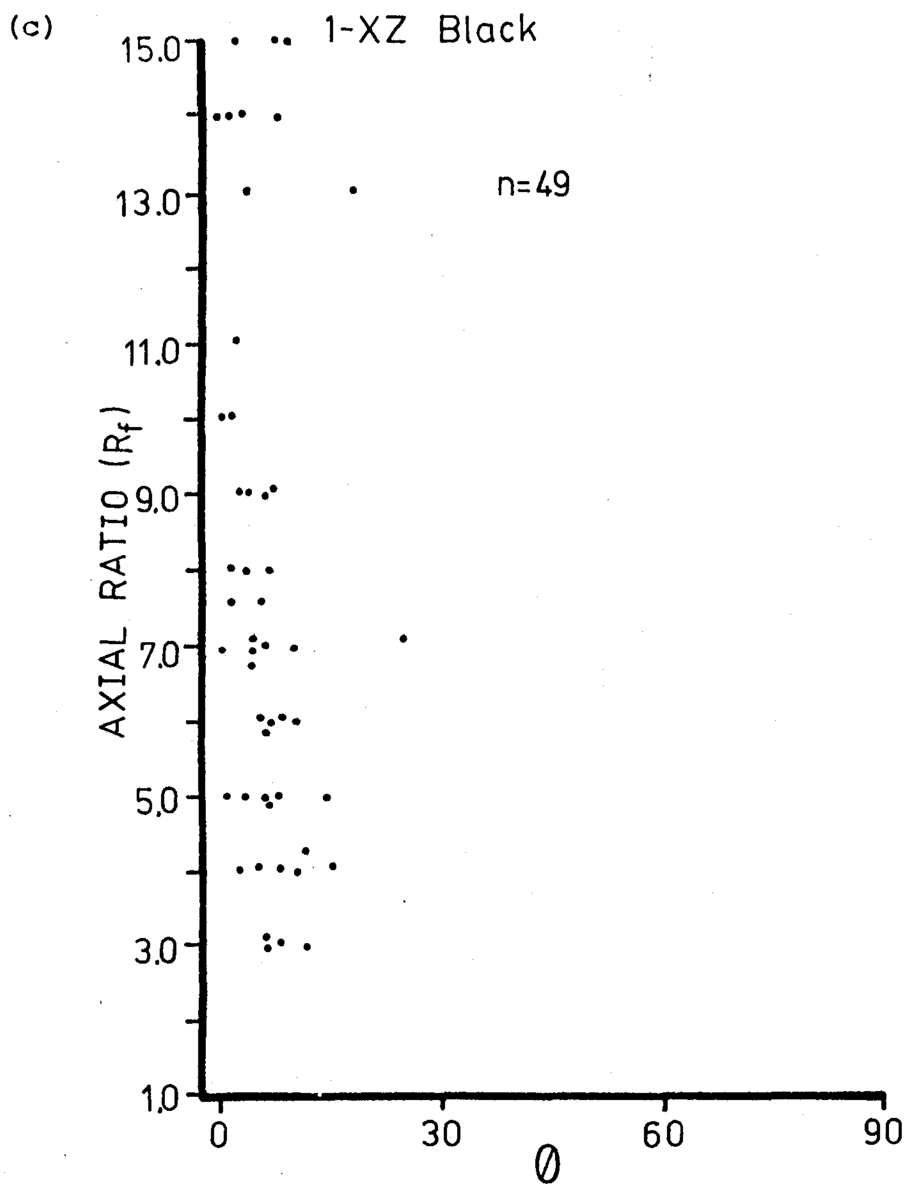
(c)
1-XZ Black
n=49
AXIAL RATIO (R_f)
15.0
13.0
11.0
9.0
7.0
5.0
3.0
1.0
0
30
60
90
Ø

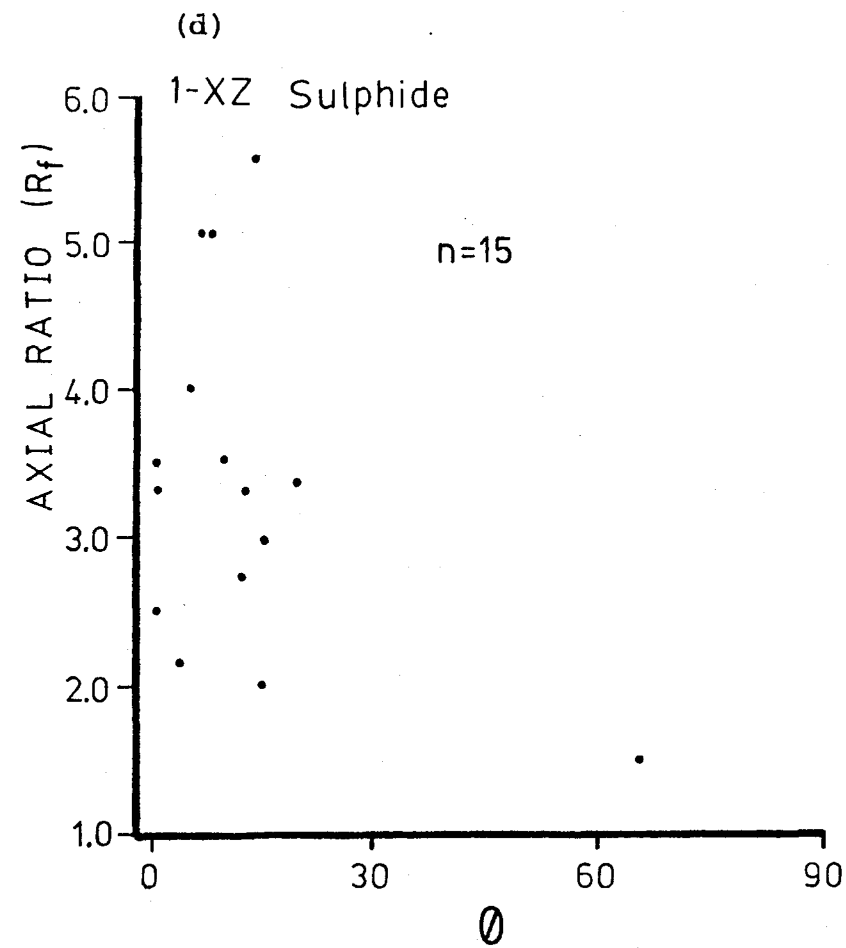
(d)
1-XZ Sulphide
n=15
AXIAL RATIO (R_f)
6.0
5.0
4.0
3.0
2.0
1.0
0
30
60
90
Ø

(e)

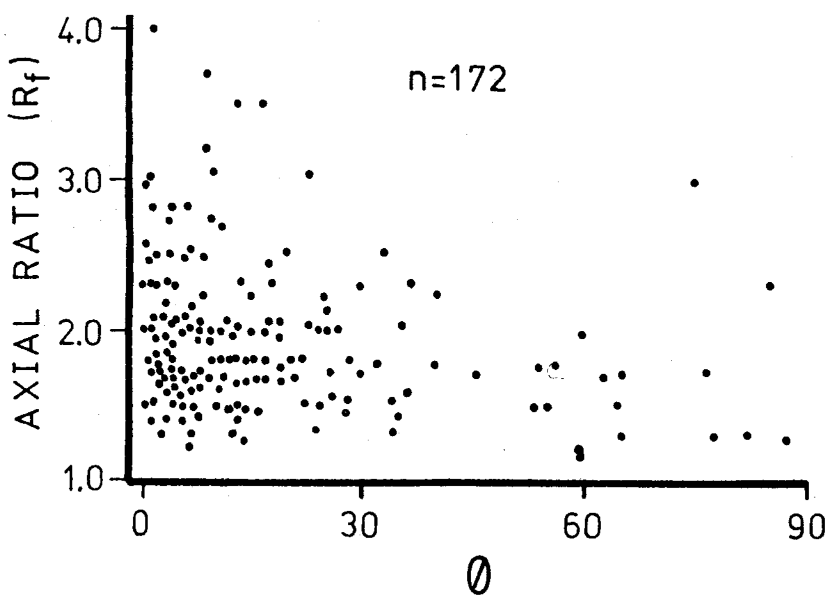
1-YZ Quartz
n=172
AXIAL RATIO (R_f)
4.0
3.0
2.0
1.0
0
30
60
90
Ø

(f)

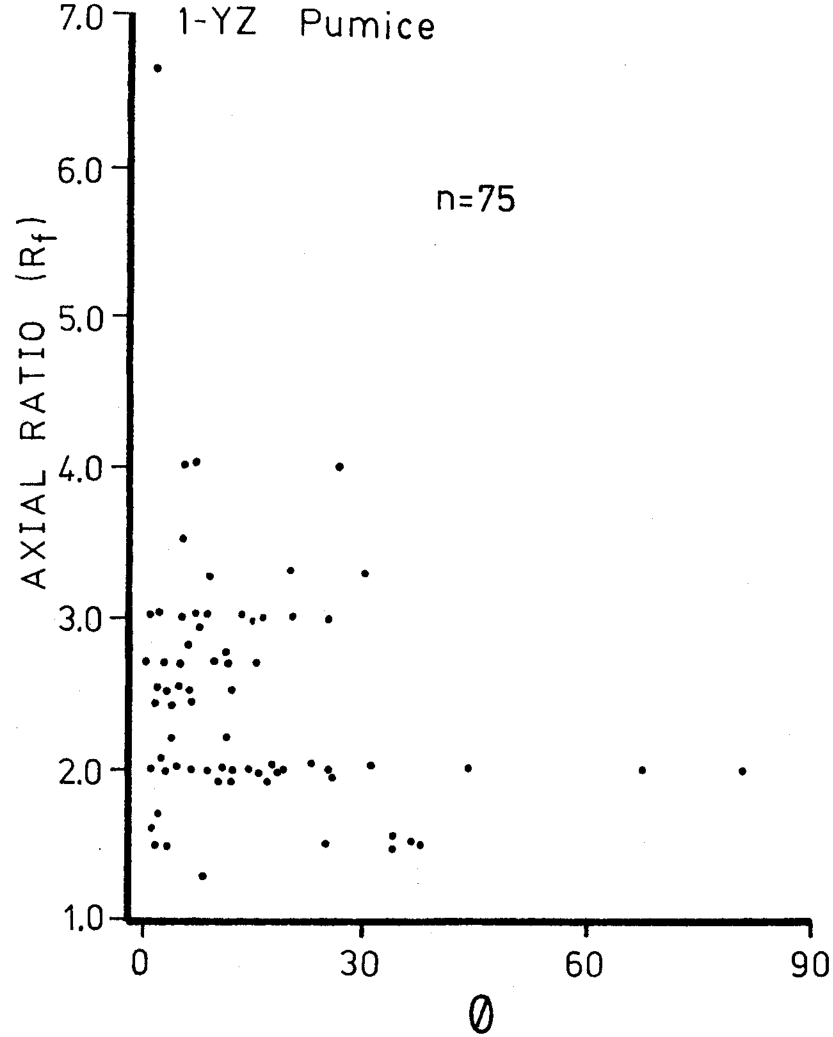
1-YZ Pumice
n=75
AXIAL RATIO (R_f)
7.0
6.0
5.0
4.0
3.0
2.0
1.0
0
30
60
90
Ø

(g)

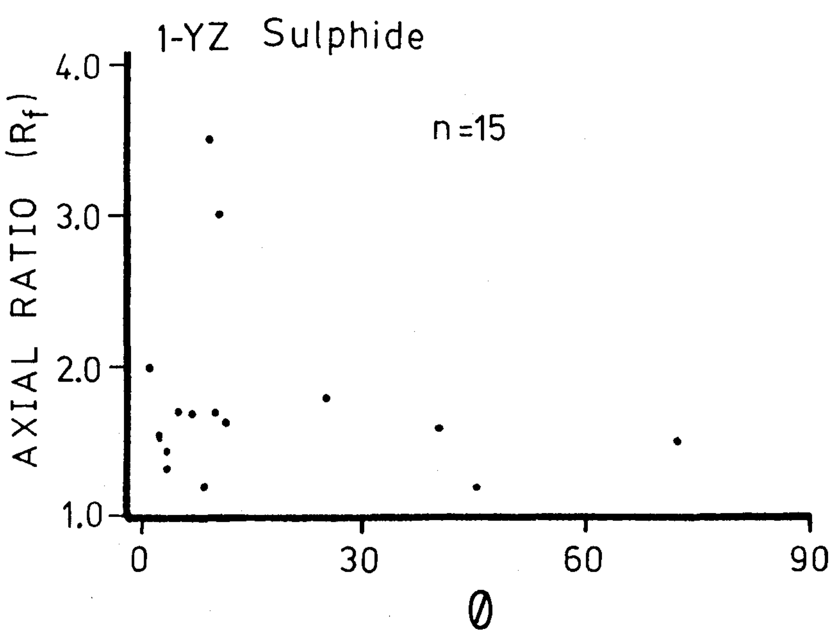
1-YZ Sulphide
n=15
AXIAL RATIO (R_f)
4.0
3.0
2.0
1.0
0
30
60
90
Ø

(h)

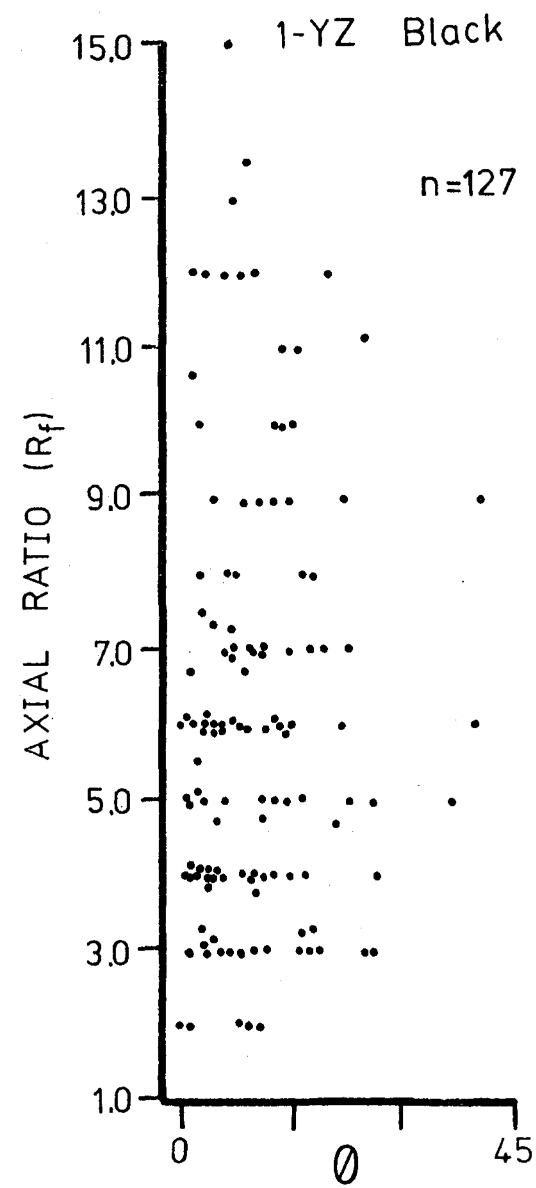
1-YZ Black
n=127
AXIAL RATIO (R_f)
15.0
13.0
11.0
9.0
7.0
5.0
3.0
1.0
0
45
Ø

Figure 4.1.1.4 a-h

R_f vs 0 diagrams for Sample 10.

(a)

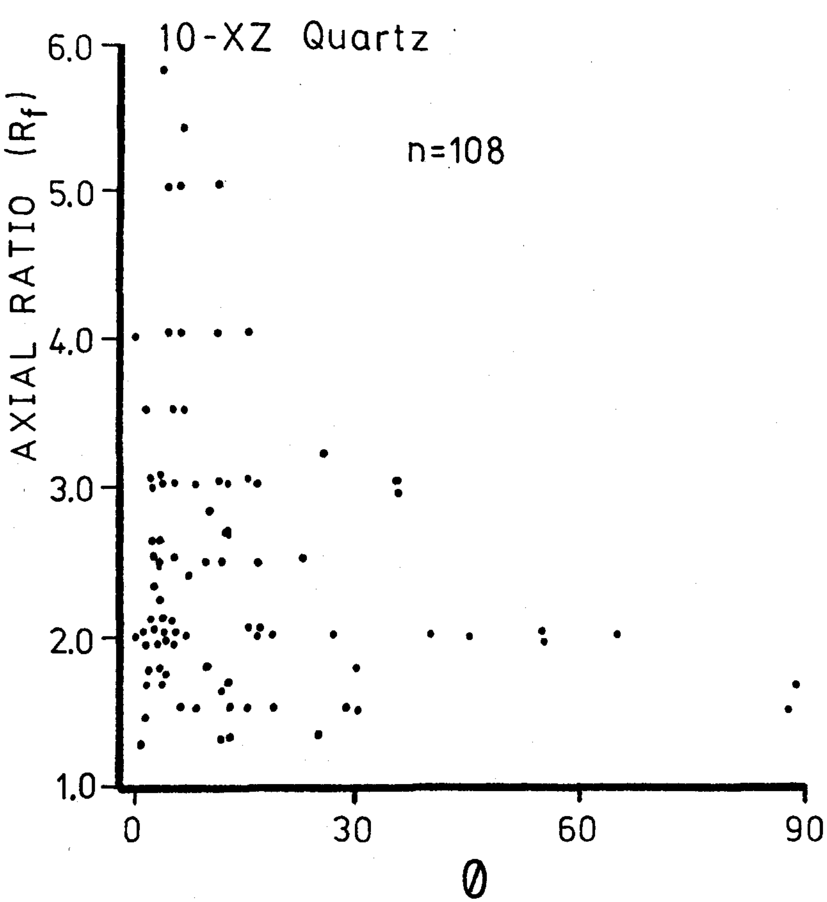
10-XZ Quartz
n=108
AXIAL RATIO (R_f)
6.0
5.0
4.0
3.0
2.0
1.0
0
30
60
90
Ø

(b)

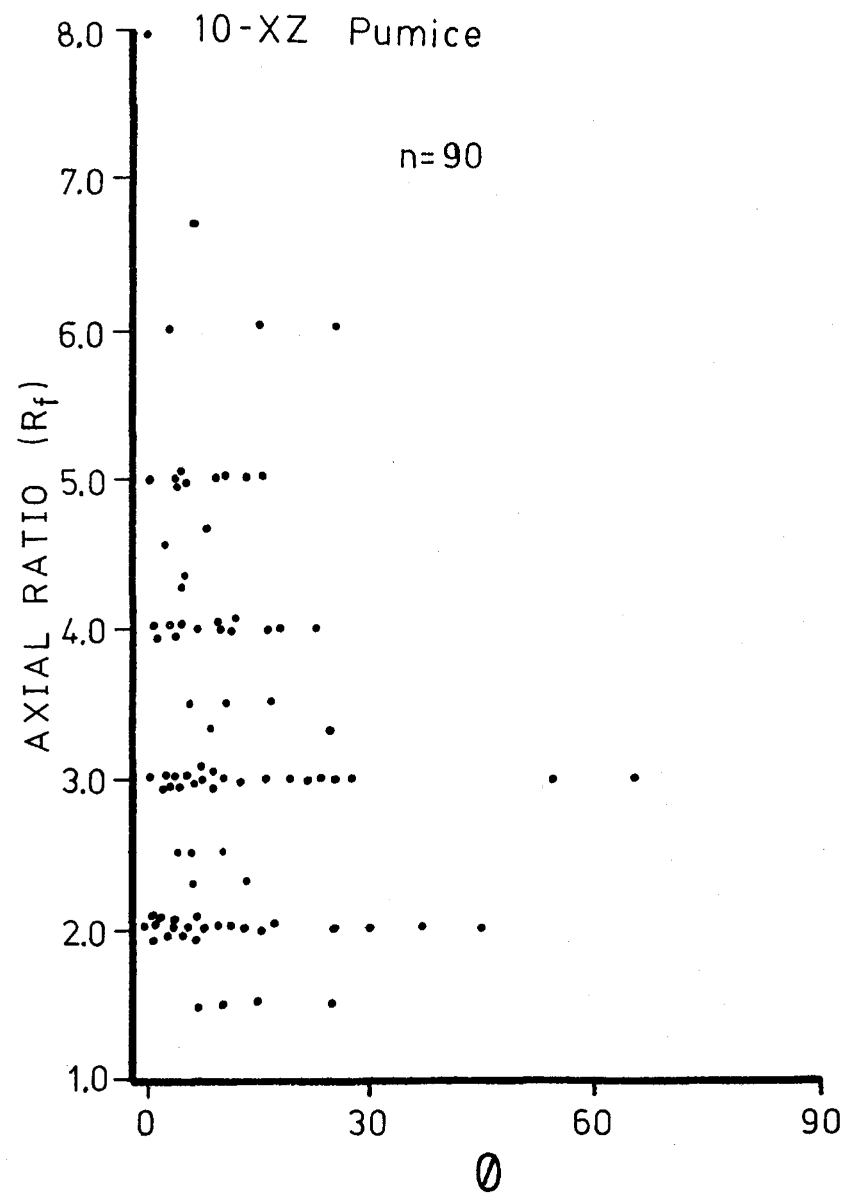
10-XZ Pumice
n= 90
AXIAL RATIO (R_f)
8.0
7.0
6.0
5.0
4.0
3.0
2.0
1.0
0
30
60
90
Ø

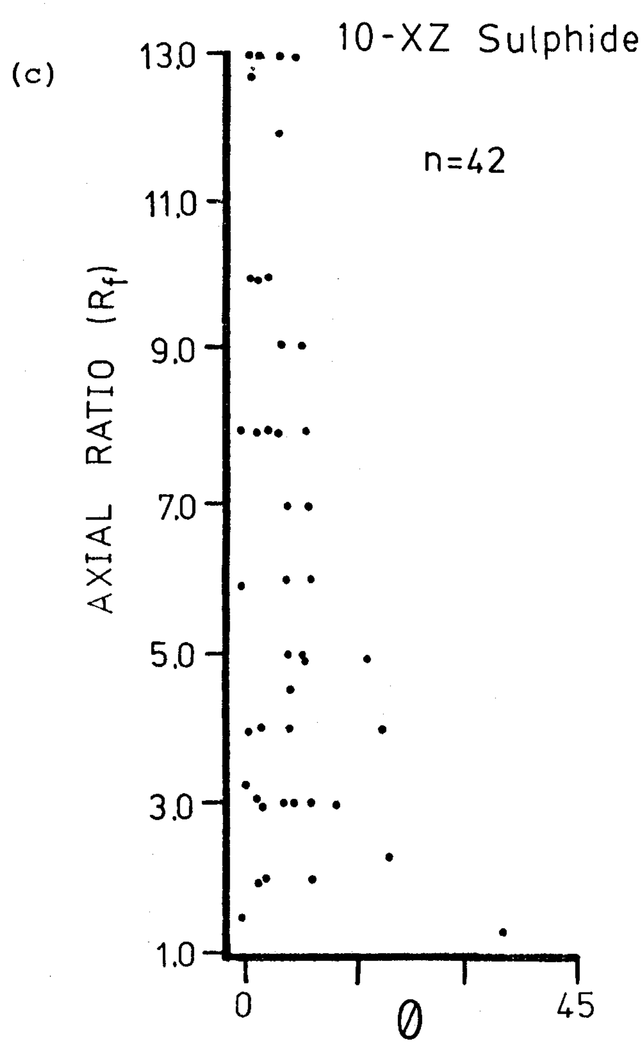
(c)
10-XZ Sulphide
n=42
AXIAL RATIO (R_f)
13.0
11.0
9.0
7.0
5.0
3.0
1.0
0
45
Ø

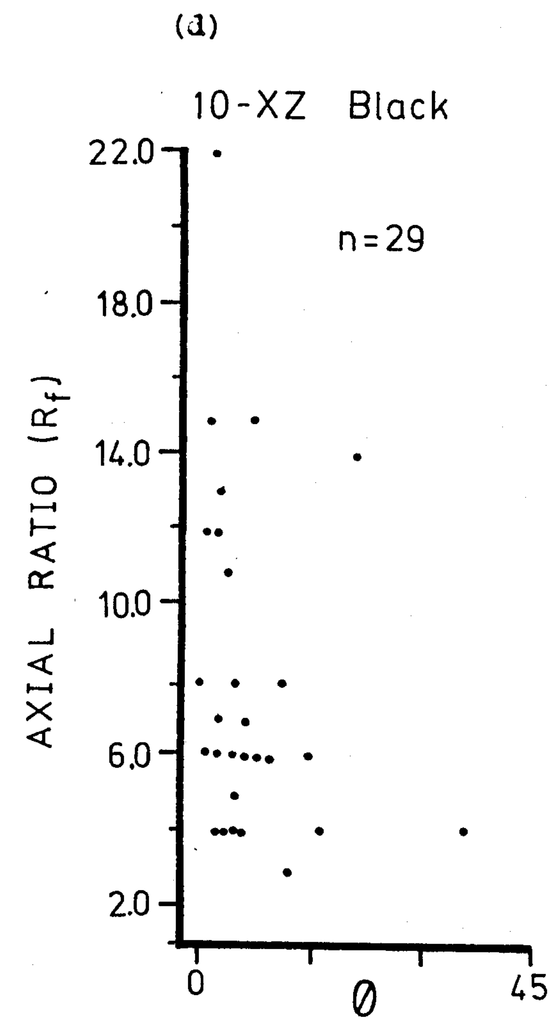
(d)
10-XZ Black
n=29
AXIAL RATIO (R_f)
22.0
18.0
14.0
10.0
6.0
2.0
0
45
Ø

(e)

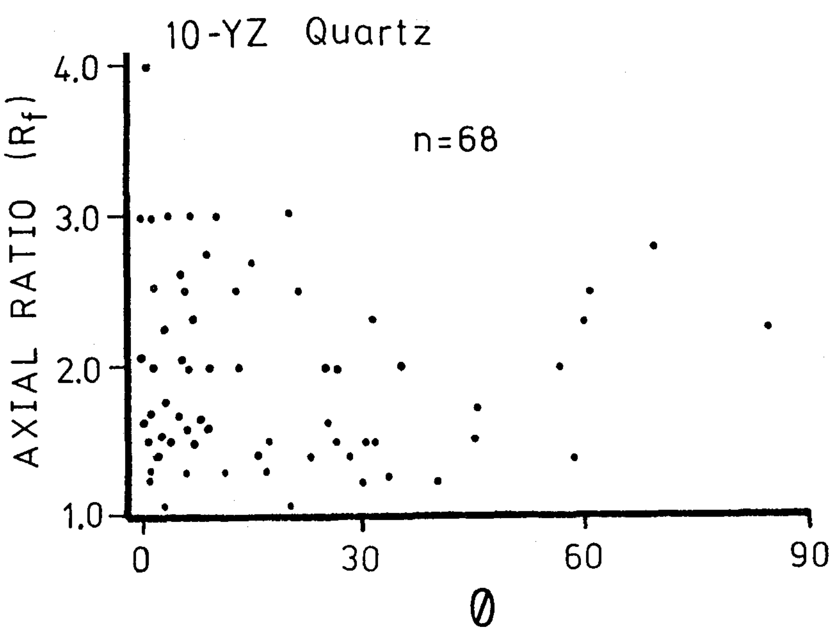
10-YZ Quartz
n=68
AXIAL RATIO (R_f)
4.0
3.0
2.0
1.0
0
30
60
90
Ø

(f)

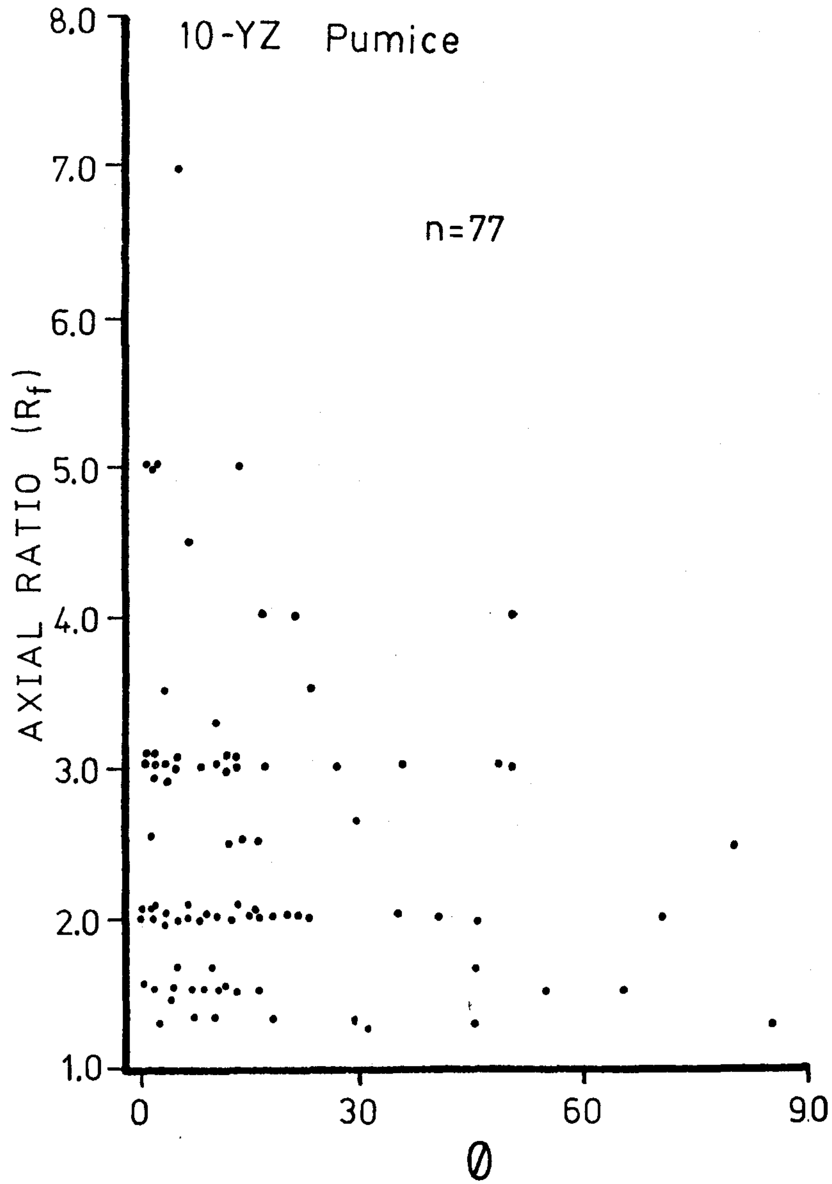
10-YZ Pumice
n=77
AXIAL RATIO (R_f)
8.0
7.0
6.0
5.0
4.0
3.0
2.0
1.0
0
30
60
90
Ø

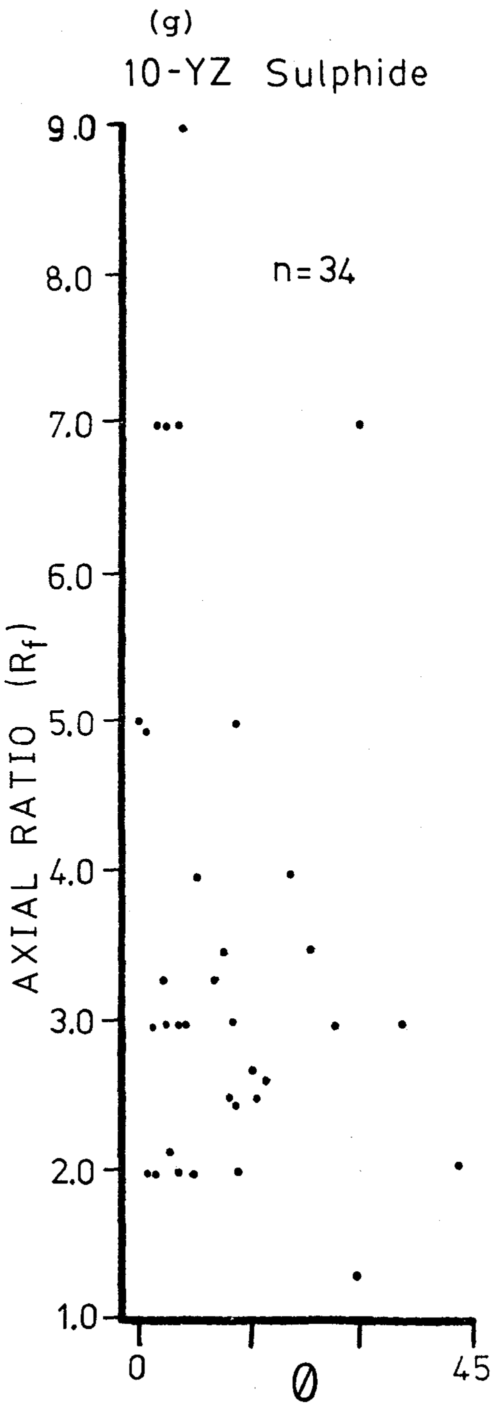
(g)
10-YZ Sulphide
n=34
AXIAL RATIO (R_f)
9.0
8.0
7.0
6.0
5.0
4.0
3.0
2.0
1.0
0
45
Ø

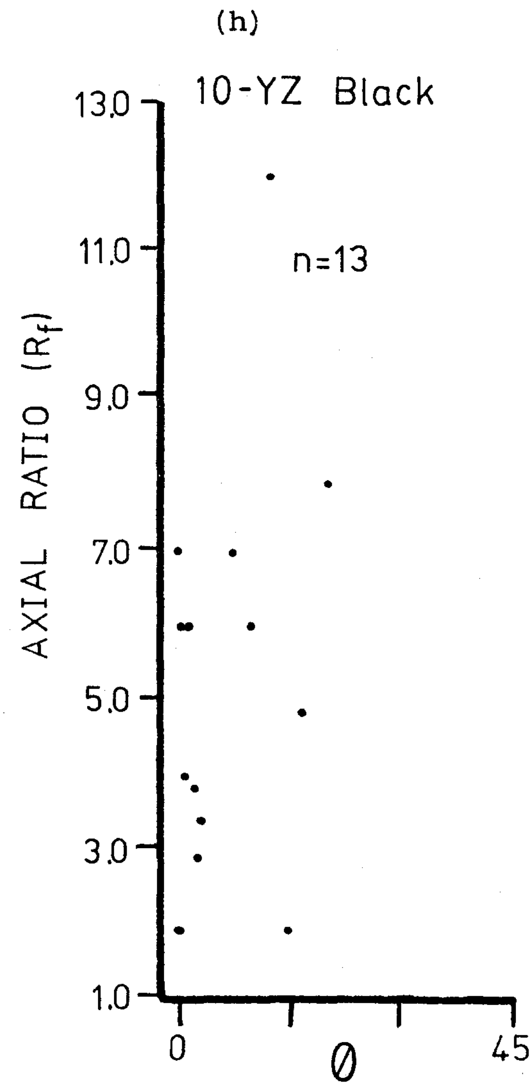
(h)
10-YZ Black
n=13
AXIAL RATIO (R_f)
13.0
11.0
9.0
7.0
5.0
3.0
1.0
0
45
Ø

TABLE 1

STRAIN VALUES CALCULATED FROM SLABS

Sample	R_s(XZ)	R_s(YZ)	Strain Ratio
4			
Quartz	2.74	2.07	1.32:1:0.48
Pumice	3.19	2.91	1.10:1:0.34
Sulphide	5.95	*5.57	1.07:1:0.17
Black	7.38	6.78	1.09:1:0.15
3			
Quartz	2.07	1.86	1.11:1:0.54
Pumice	2.89	2.52	1.15:1:0.40
Sulphide	7.15	2.44	2.93:1:0.41
Black	10.65	6.78	1.62:1:0.15
1			
Quartz	2.08	1.83	1.14:1:0.55
Pumice	2.06	1.62	1.27:1:0.62
Sulphide	3.17	1.55	2.05:1:0.65
Black	7.13	5.51	1.29:1:0.18
10			
Quartz	2.05	1.64	1.25:1:0.61
Pumice	2.66	1.75	1.52:1:0.57
Sulphide	5.04	3.08	1.64:1:0.32
Black	6.61	4.63	1.43:1:0.22

*Calculated from limited data

4.1.2 Flinn Diagram

The Flinn diagram is virtually a deformation plot. The shapes of strain ellipsoids can be plotted on rectangular co-ordinates by using the ratios of their axes (Flinn 1962). The natural logarithms of the ratios of X/Y and Y/Z are plotted on the ordinate and the abcissa respectively (Ramsay 1967). The origin of the graph represents a sphere and every other point on the graph represents an ellipsoid with a specific shape.

The graph can be contoured with straight lines radiating from the origin (Flinn 1956). These lines represent pseudo-deformation paths. The k=1 line represents deformation whereby the strain is plane strain and there is no volume loss. All ellipsoids that plot below the k=1 line are in a "flattening type" deformation field, while ellipsoids located above the k=1 line are in a "constriction type" deformation field.

The strain ellipsoids for each clast family at each sample location in the coarse basal section of the unit are shown on the Flinn plot (Figure 4.1.2). In the pumice, black, and sulphide clasts, there is a change from a flattening type deformation toward a constriction type deformation moving vertically up through the unit. The quartz clasts do not show this type of change.

Almost all the points lie in the field of apparent flattening. The only points located in the apparent constriction field belong to the sulphide clast family.

Figure 4.1.2

Flinn Plot

o Quartz

• Pumice

× Sulphide

▵ Black

The arrows point in the direction from the base of the unit towards the top.

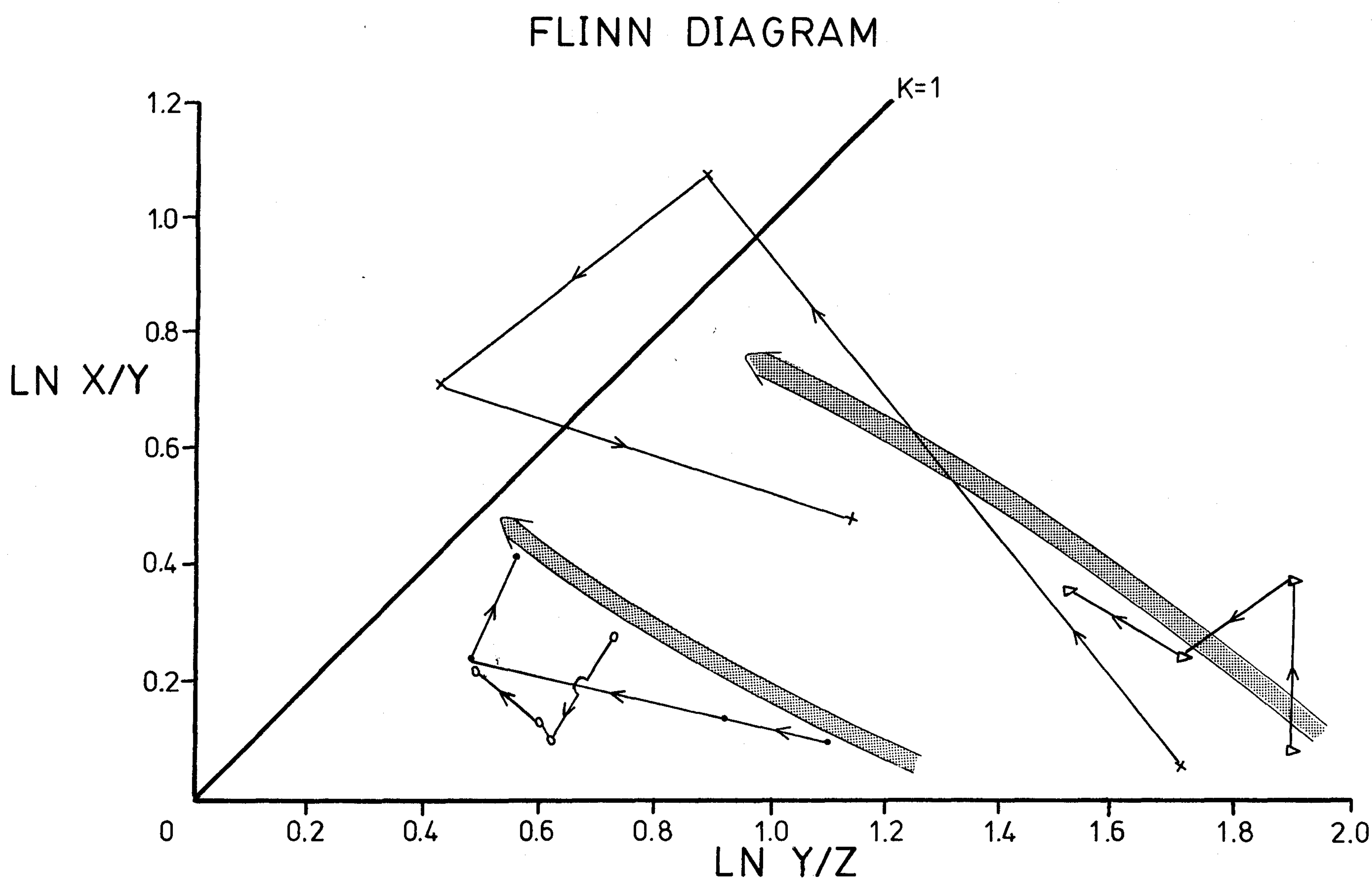
FLINN DIAGRAM
K=1
LN X/Y
LN Y/Z
1.2
1.0
0.8
0.6
0.4
0.2
0
0.2
0.4
0.6
0.8
1.0
1.2
1.4
1.6
1.8
2.0

4.2 Grain Size Analysis

4.2.1 Grain Size vs. Vertical Position in the Unit

The grain size variation in the coarser basal section of the deposit was measured to give two kinds of data. First, the mean grain diameters were calculated for each clast family at each of the sample sites. The results are shown in figure 4.2.1(a) and table 2. Second, field measurements of maximum clast size were made at six positions in the outcrop. The results are shown in figure 4.2.1(b) and table 2. The prominent feature shown in these graphs is the presence of reverse to normal grading of mean grain size of the pumice, black and sulphide clasts. The maximum clast size, measured in the field, does not occur at the base of the deposit. The grading in the maximum clast size measurement is reversed to normal. The quartz clasts, measured from the slabs, are the only clasts that show normal grading of mean grain size through the entire basal section of the unit. The quartz clast grading is approximately linear with height in the sequence.

The grain size variation in the fine grained top section of the unit was measured using thin sections. The measurements were restricted to the pure quartz grains. The results are shown in figure 4.2.1(c) and table 2. The graph shows a normal grading of the quartz grains (clasts) in the top fine grained section of the unit.

Figure 4.2.1

Grain size vs verticle position in the unit.

a) Average clast diameter (mm) from slab data.

Q - Quartz

P - Pumice

S - Sulphide

B - Black

b) Maximum clast diameter (mm) from field data.

c) Maximum quartz grain diameter (mm) from thin section data.

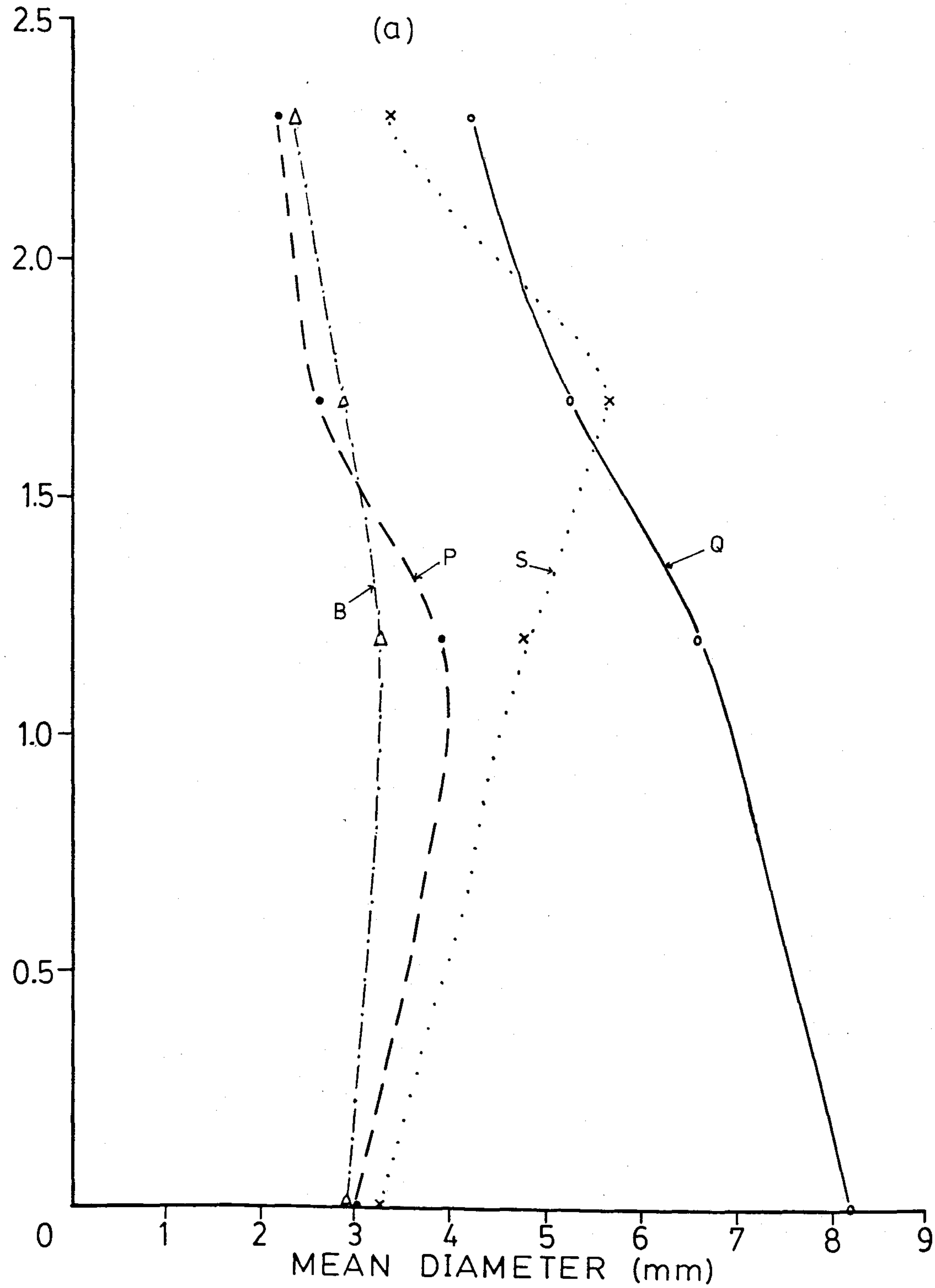
(a)
2.5
2.0
1.5
1.0
0.5
0
1
2
3
4
5
6
7
8
9
MEAN DIAMETER (mm)
P
Q
S
B

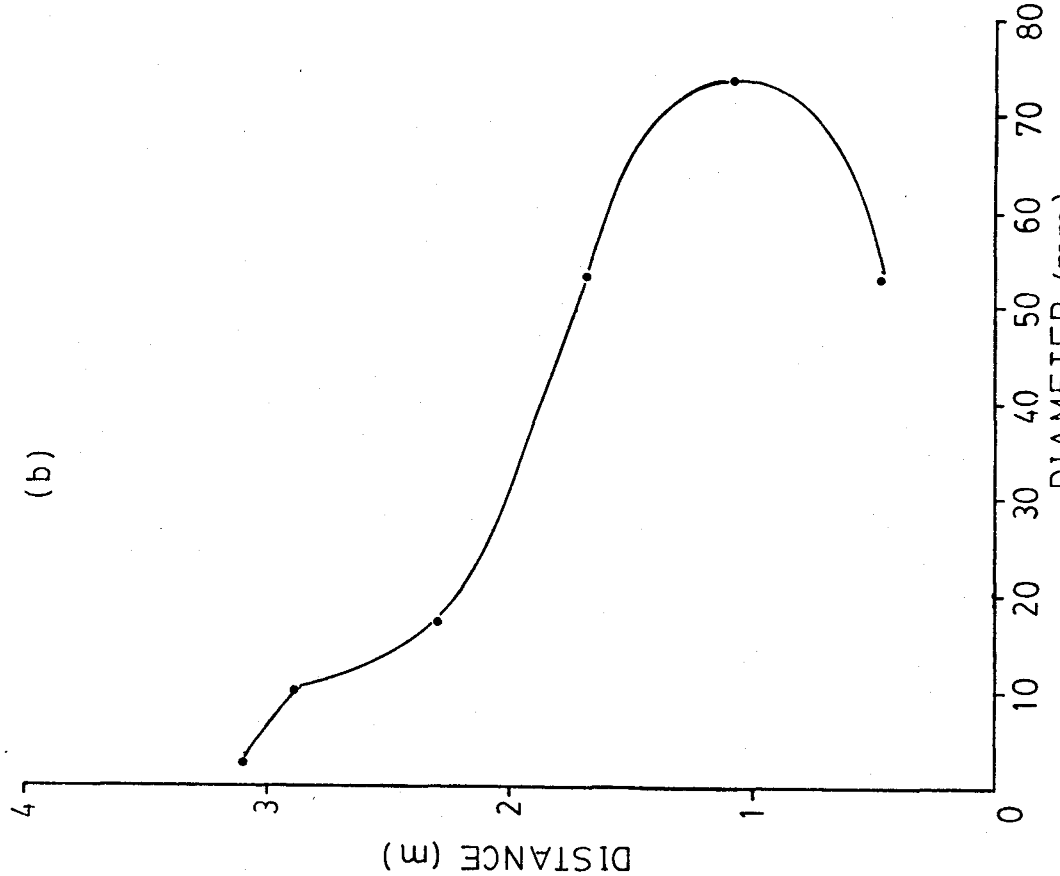
(b)
DISTANCE (m)
DIAMETER (mm)
0
1
2
3
4
10
20
30
40
50
60
70
80

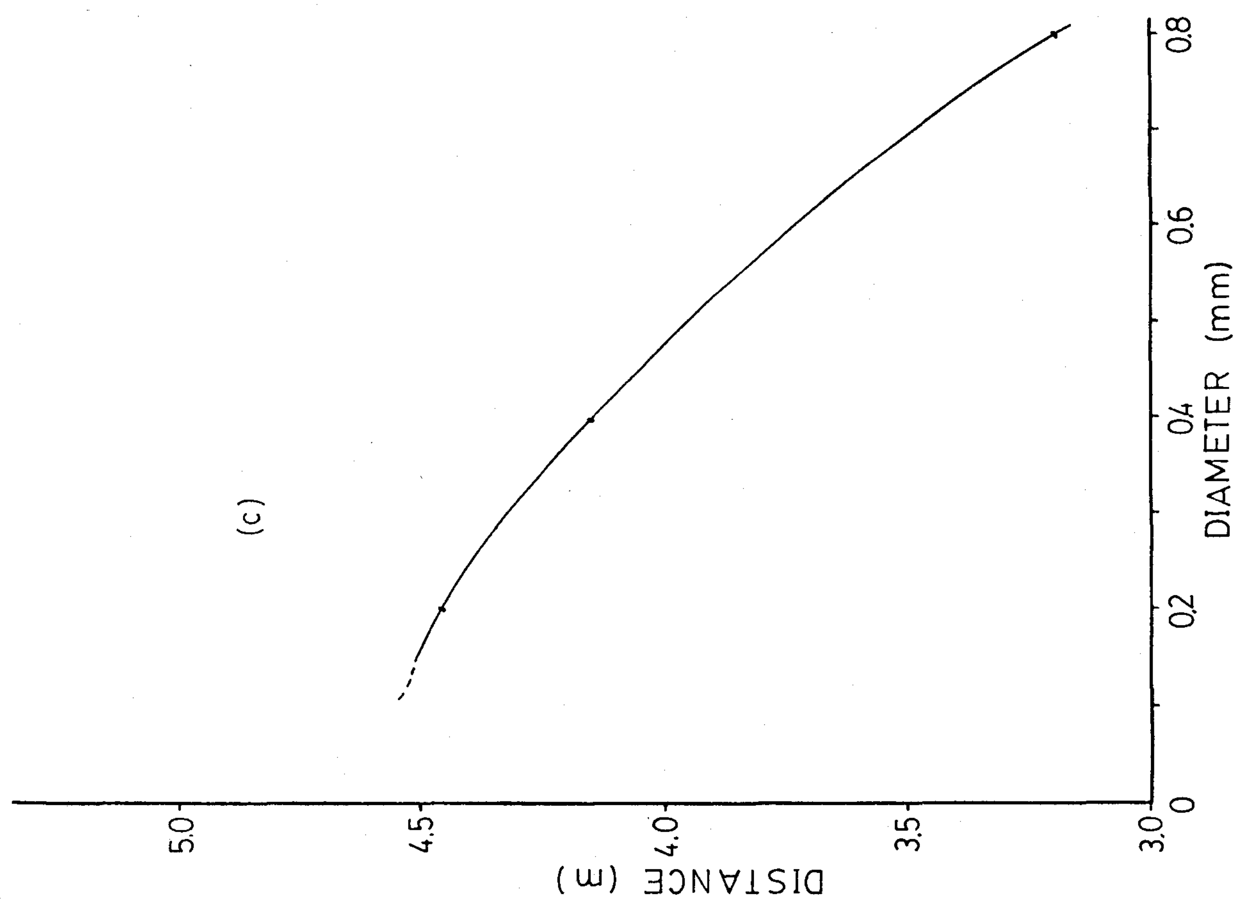
(c)
DISTANCE (m)
DIAMETER (mm)
3.0
3.5
4.0
4.5
5.0
0
0.2
0.4
0.6
0.8

TABLE 2

VARIATION IN CLAST SIZE WITH LOCATION IN OUTCROP

DISTANCE ABOVE BASE (Meters)	SAMPLE NUMBER	AVERAGE CLAST DIAMETER (mm) (Slab Data)				MAXIMUM CLAST DIAMETER (mm) (Field Data)	MAXIMUM QUARTZ GRAIN DIAMETER (mm) (Thin Section Data)
		QUARTZ	PUMICE	SULPHIDE	BLACK		
TOP 5.3--	2						not seen
5.0--							
	6						0.2
	5						0.4
4.0--							
	13						0.8
						2	
3.0--						10	
	10	4.2	2.2	3.3	2.4	17	
2.0--							
	1	5.2	2.6	5.7	2.8	53	
	3	6.6	3.3	4.8	3.3		
1.0--						74	
						53	
BASE 0.0--	4	8.2	3.0	3.3	3.0		

4.2.2 Cumulative Frequency Curves

The grain size data used are from measurements from slab surfaces. In calculating these curves, all the clasts smaller than 0 phi are assumed to be matrix. Below this grain size the measurement of the grains is difficult because the grain boundaries are not distinctly seen in the slabs. Therefore, the graphs represent only the coarse fraction of the deposit. The measured dimensions of the clasts in slabs will differ from the true dimensions of the clasts due to the random sectioning through the clasts. No one has yet found a method to convert sorting values derived from slab measurement techniques to those of sieving techniques. However, Friedman (1958) noted that the discrepancy between the cumulative frequency curves from slab measurements and sieving measurements is small and that the two techniques are related in a linear fashion. The cumulative frequency curves will show sorting values to be poorer than they actually are. However, the relative sorting values between curves can be approximated using the orientations of these curves. A curve that represents a well sorted clast family will be steeper than a curve representing a poorly sorted clast family. Mean grain sizes can be compared between curves by using the relative positions of the cumulative frequency curves. A curve representing a coarse clast family will be located to the left, or the low phi, side of the graph compared to a curve that respresents a fine clast family.

Each of the graphs in figures 4.2.2(a) to 4.2.2(d) represents one of the samples from the basal section of the unit. Each clast family is represented by a curve on these graphs. All the samples show quartz to be the most poorly sorted clast family followed by the sulphide clast family. The pumice and black clasts are consistently the best sorted clasts. The mean grain sizes seem to vary in a similar manner as the sorting. The quartz clasts are typically the coarsest clasts followed by the sulphide clasts. The pumice and the black clasts are the finest grained clast families.

Figure 4.2.2(e) is a graph showing the curves calculated for each sample using all the clast families. This graph shows that the sorting improves slightly, upward through the unit, and that the mean grain size of the coarse (Ø>0) fraction decreases.

Figure 4.2.2

Cumulative Frequency Curves

a) Sample 4

b) Sample 3

c) Sample 1

d) Sample 10

Q - Quartz

P - Pumice

S - Sulphide

B - Black

e) All clasts

(a)

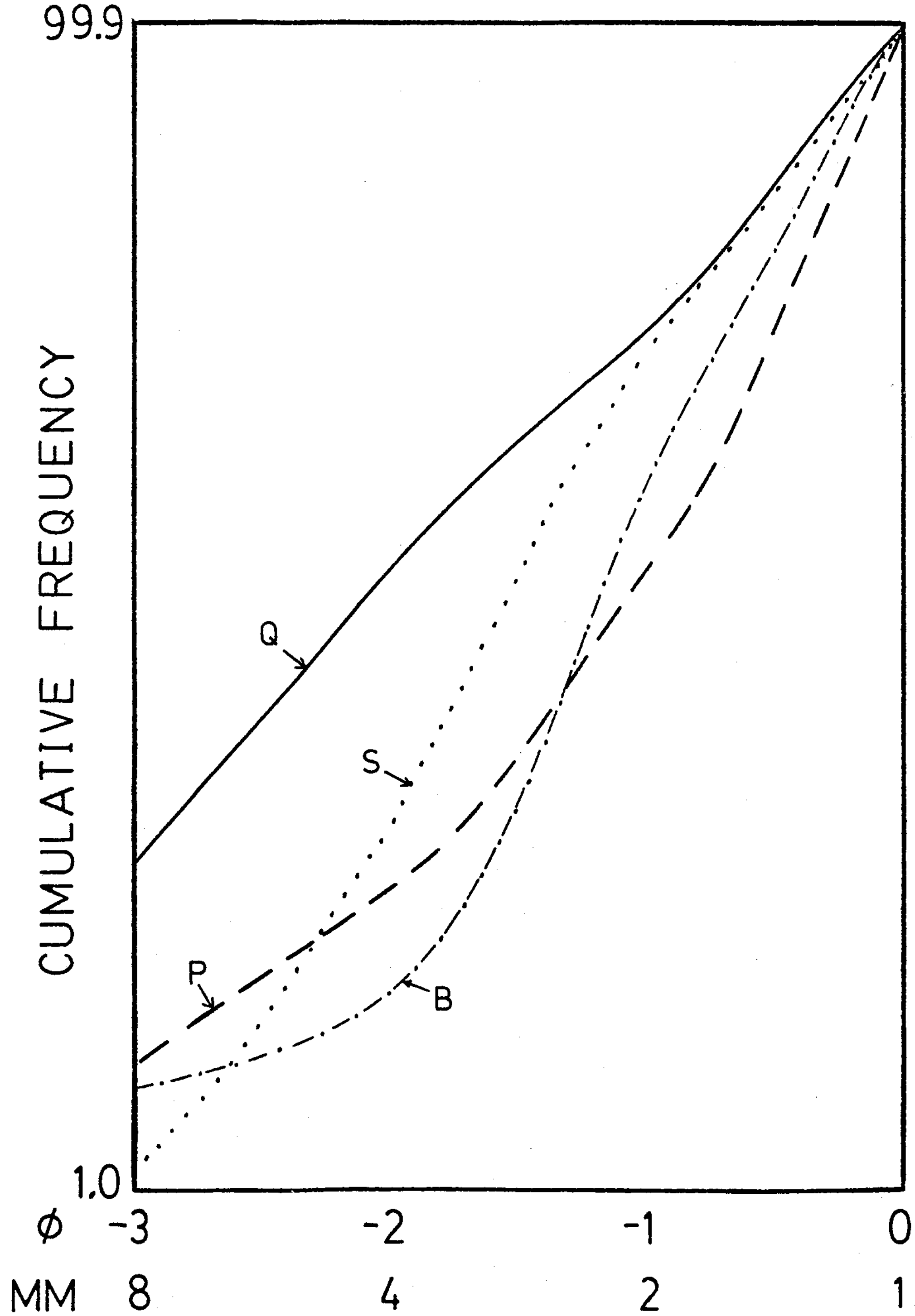

(b)

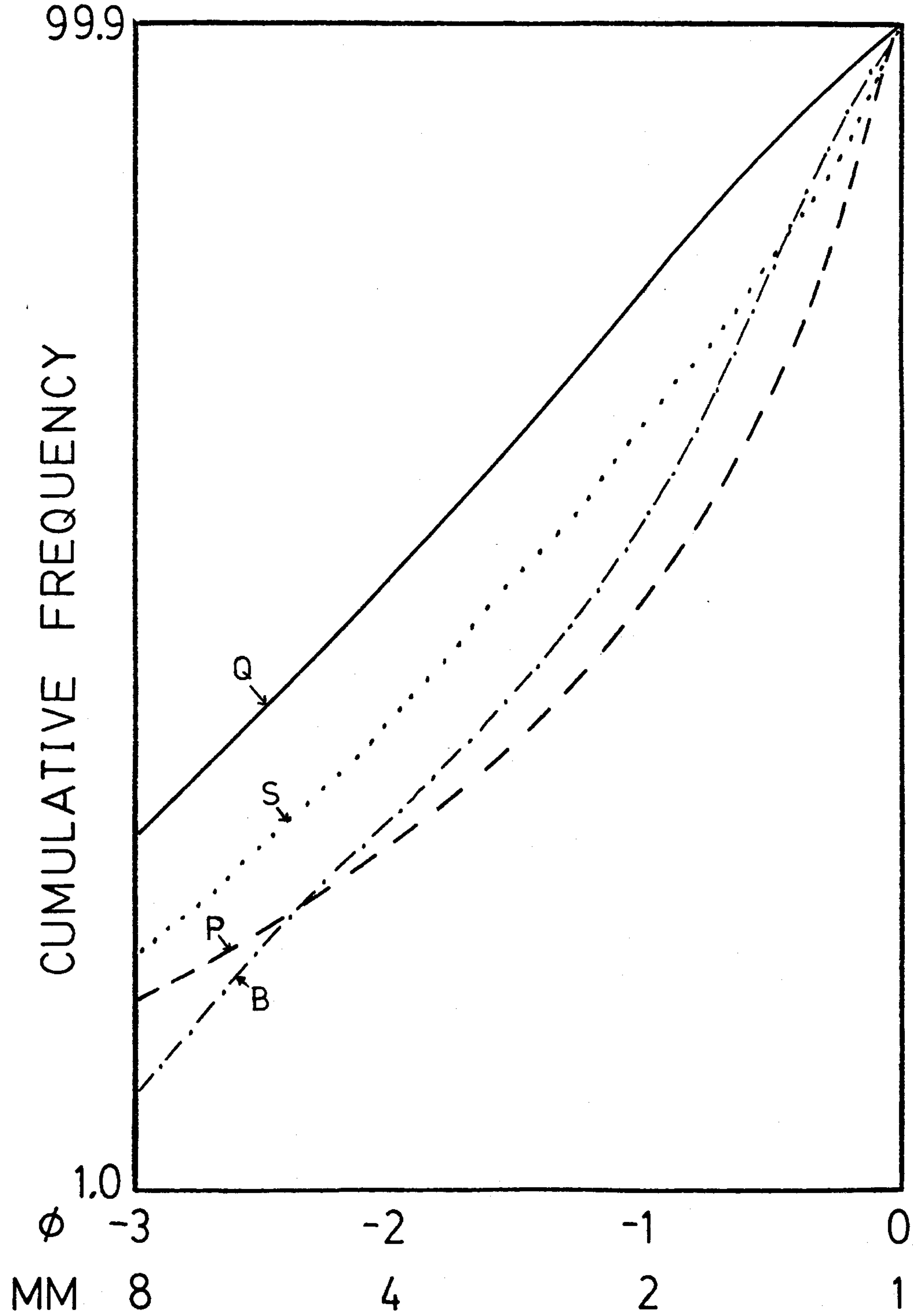

(c)

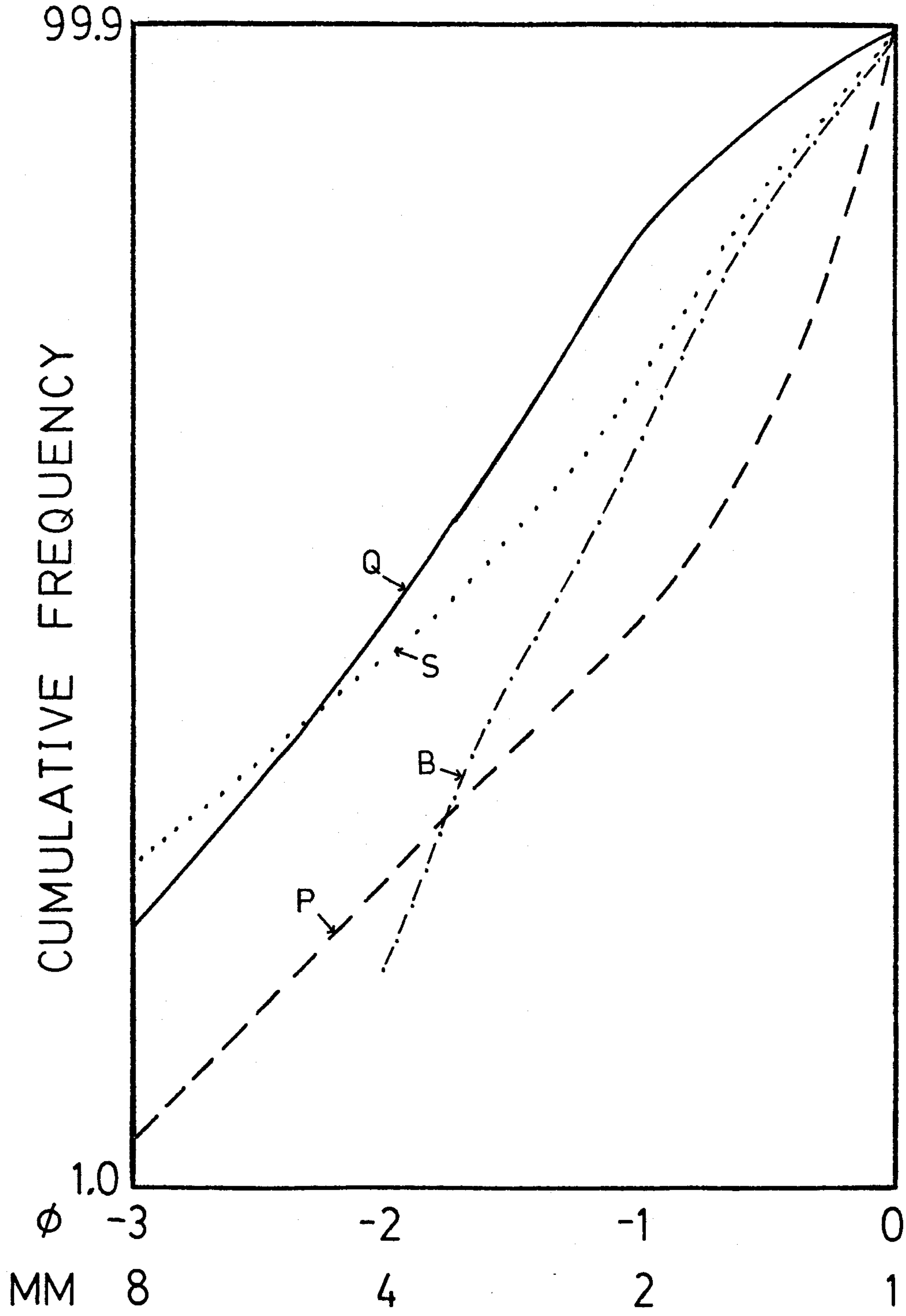

(d)

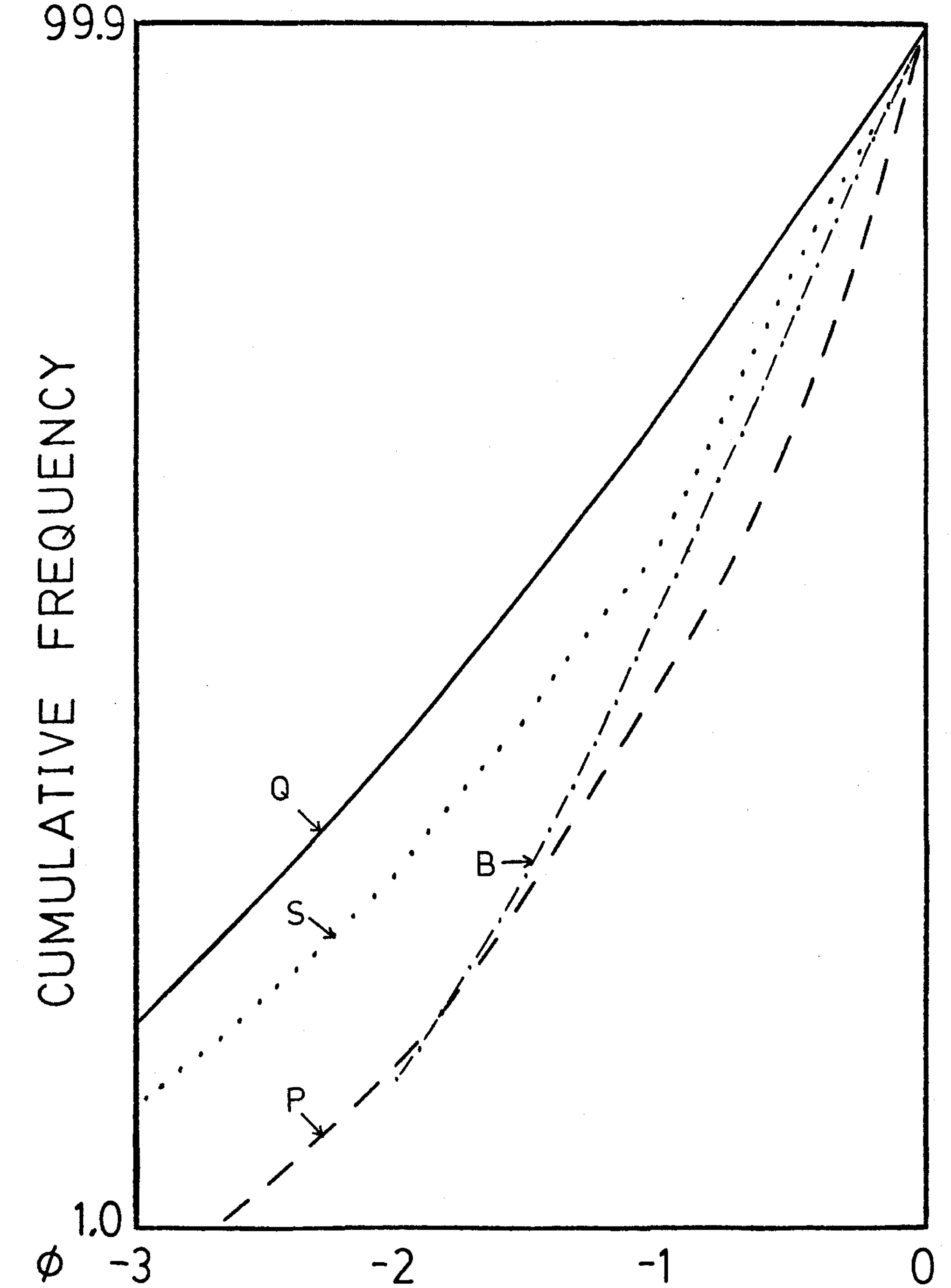

(e)

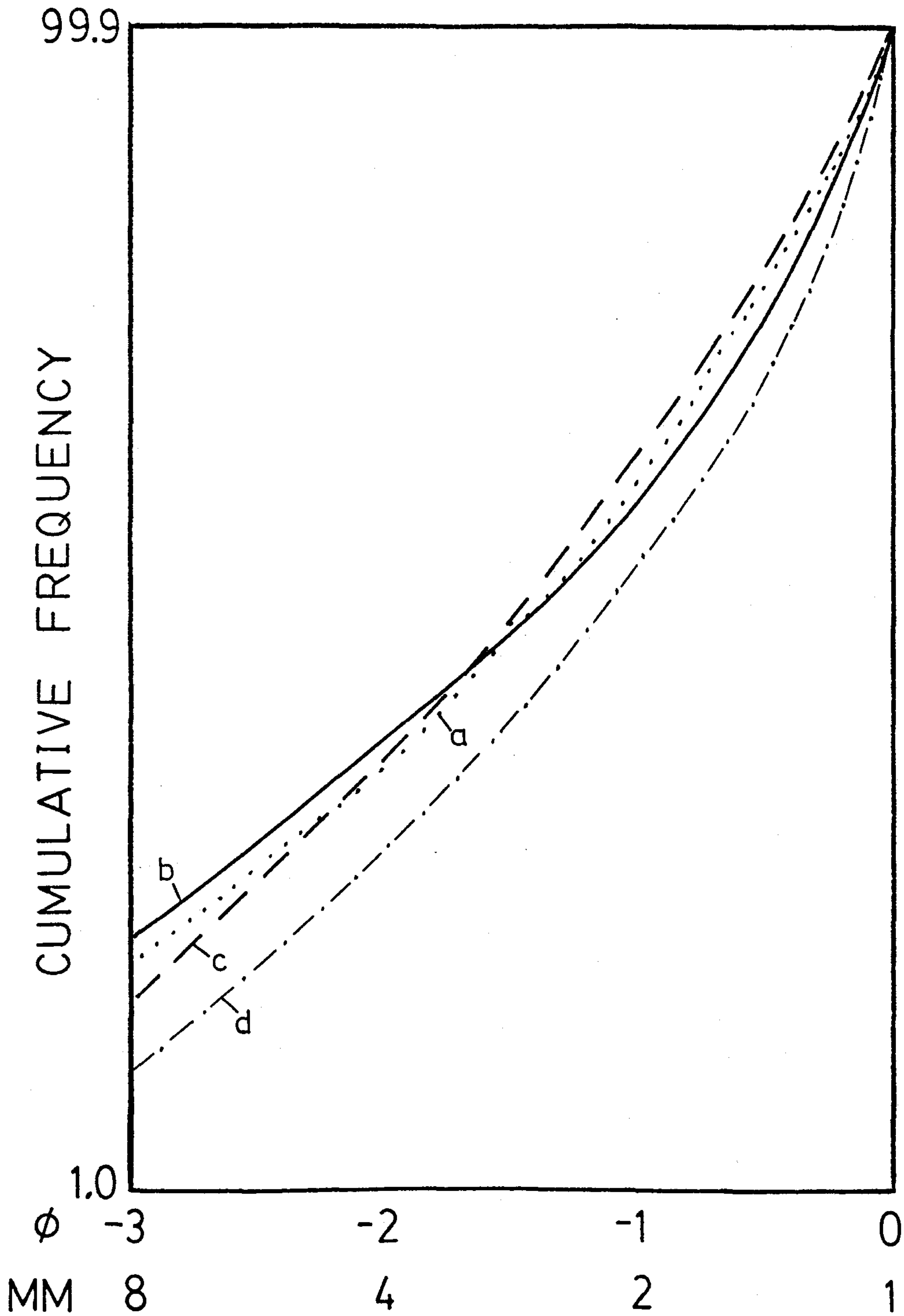

CHAPTER 5

INTERPRETATION

5.1 Effect of Strain on the Clasts

The use of the strain data to interpret an original sedimentary fabric using the method described by Dunnett and Siddans (1971) is not possible because the orientation of one of the principal planes of strain (XY) is parallel to the bedding plane. This suggests irrotational strain. However, the quartz clasts have a fluctuation angle that is generally greater than 90°. These measurements come from sections that are oriented normal to bedding and have the highest tectonic strain ratios. If there was an originally preferred orientation of the clasts this preferred orientation would occur in these sections. The presence of the high fluctuation angle indicates strongly that the original orientation of quartz clasts, and probably all other clasts, was completely random.

The difference in the strain ratios and the fluctuation angles between clast families can be interpreted as a result of the differences in their viscosity ratios between the clasts and the matrix. The quartz clasts, which have a viscosity ratio nearing unity, are the least strained clast family and probably represent the strain in the rock as a whole. The pumice clasts have strain ratios slightly higher than the quartz clasts. This is a result of the pumice clasts having a lower viscosity than the quartz clasts. The lower viscosity of the pumice clasts is a result of the pumice containing vesicles and having an original composition different from that of the quartz. This variation in strain between different clast lithologies has been noticed by several people, including Hsu (1971) and Gay (1967). The high strain ratio in the sulphide clasts is probably more the result of recrystallization of the sulphide as opposed to the sulphide having a low viscosity ratio. The highest strain ratio is exhibited in the black clast family. This is interpreted as being a result of the black clast family having a very low viscosity or being due to a secondary crystallization of the micaceous material in the areas of the black clasts, or both.

The deformation levels, as shown in the Flinn diagram results, indicate that some of the flattening of the pumice, black and sulphide clasts occured during the initial deposition of the unit. The change toward more flattening from the top to the base of the lower section of the deposit could be interpreted as initial compaction occuring immediately after or during the depositional process. The compaction would be the result of a downward pressure of the material within the unit. This type of compaction would be expected to cause more flattening in the lower portion of the deposit. Obviously the clasts which would show this compaction effect would have to have low viscosities while the clasts with high viscosities would not be deformed by this process. This is shown particularly while by comparing the deformation plots of the easily compacted pumice clasts to the more viscous quartz clasts. The quartz clasts do not show any effect of compaction while the pumice clasts do. Fisher and Schmincke (1984) noted that large pumice clasts in the massive parts of submarine pyroclastic flows tend to be randomly oriented except toward their base, when the elongation is parallel to the contacts. Plate 3(A) shows a pumice clast that is being bent about a more viscous quartz clast. A similar change toward more flattening is noticed in the black and sulphide clasts. These changes could be interpreted in a similar manner as the pumice clasts. The sulphide behaviour is questionable because the sulphide clasts enter the constriction type deformation field. Also, the sulphides may have a switch in the orientations of the X and Y axes of strain in section 4. Both these facts imply that the sulphide clasts reacted differently to the strain than the pumice and quartz clasts reacted. Recrystallization of the sulphide is probably occuring as implied by the very hig strain ratios and by the textures noted in section 2.4.2.

5.2 Grain Size Analysis

The variation in grain size and sorting between clast families and the position in the deposit will help in the interpretation of the mode of deposition of the deposit.

At any one sample site, the differences in the mean grain sizes of the clast families cannot be interpreted as being a result of hydraulic sorting. Hydraulic sorting is a possible interpretation of the differences in the quartz and sulphide clast sizes since the denser sulphide clasts always have mean clast diameters smaller than that of the quartz clasts. The pumice clasts are consistently the finest grained. This could be due to flotation of the pumice and is indeed not due to normal hydraulic sorting because pumice has a very low density. The higher degree of sorting of the pumice clasts relative to the quartz clasts and the sulphidé clasts could be due to this flotation effect.

Within the massive coarse grained division of the unit, the presence of normal grading of the mean quartz clast diameter and reverse to normal grading of the mean pumice clast diameter supports the idea of flotation of the pumice clasts. Lajoie (1984) mentioned that the pumice clasts would tend to float within a denser matrix of the flow. Therefore, the flotation of the pumice clasts can occur in a density flow.

The maximum clast size did not occur at the base of the deposit. This feature has been noticed by Yamada (1973) in a subaqueous debris flow.

The massive basal division of the deposit has poor sorting, lacks stratifications, and there is evidence that there was an original random orientation of the clasts (section 5.1). These features are all common in subaqueous debris flow deposits described by Fisher and Schmincke (1984). This implies that the deposit was a result of a debris or density flow as opposed to being fluid driven.

The improvement in sorting from the base to the top of the massive unit could be interpreted as being a result of increasing effect of the water on the density flow; a form of elutriation.

The overall grading of the deposit continues through the fine division to the top of the unit. This implies that the entire deposit was emplaced during one event.

5.3 Relation to Subaqueous Pyroclastic Flows

The deposit is interpreted as a subaqueous volcanic debris flow because of the presence of pumice clasts in the unit and pillowed basalts enclosing the unit. Similar deposits have be studied in Japan by Fiske and Matsuda (1964) and in the Noranda region, Quebec by Tasse et al (1978). The Japanese deposits are interpreted as being deposited in a subaqueous environment because they are interbedded with fossiliferous marine mudstones. The depoits in the Noranda area are also interpreted as being deposited subaqueously because they are interbedded with pillowed flows. Fisher and Schmincke (1984) have summarized these types of deposits.

Subaqueous pyroclastic flows are characterized by the presence of two divisions within the depositional unit; a lower coarse grained massive bed composed of lapelli-tuff and a fine grained thinly bedded top of similar composition.

The lower division commonly composes over half the thickness of the unit. The lower division is one massive bed which is coarse grained, poorly sorted, lacks internal stratification and has normal grading of the lithice and reverse grading of the pumice clasts. Fiske and Matsuda recognized clasts up to -4Ø and Tasse et al recognized clasts as large as -10Ø. All these features are recognized in the deposit in the Temagami area.

The top division is much finer grained and textures within this division are best described by Fiske and Matsuda (1964) because the deposits in Japan are Miocene in age. The top division is characterized by the presence of many thin beds of fine grained silt and clay sized material. The division contains two types of grading.

Each individual bed is normally graded and the entire top division is normally graded. The grading in each bed is defined by a density grading and the mean grain size may also grade normally or remain nearly uniform through the bed. The deposit under study has a laminated top division composed of fine grained silicic material. There is no evidence of individual graded beds in the top division unless the laminations in the top division represent bedding proper. The thin sections do not show an size graduation between the laminations but this is not necessarily require because the grading described by Fiske and Matsuda (1964) is mostly a density grading.

The presence of clasts the size of cobbles (-6Ø) and the angularity seen in some of the clasts is indicative that this deposit was derived from an accumulation proximal to the volcanic source. Tasse et al (1978) mentioned that debris flows are more common in a proximal environment and turbulent flow are more common in a distal environment. The fact that there are no stratifications in the massive division of the deposit also implies that the unit under study is located in a proximal environment.

CHAPTER 6

CONCLUSIONS

The presence of an original sedimentary fabric could not be determined by methods described by Dunnett and Siddans (1971) because the bedding is oriented parallel to one of the principal planes of strain. This results in irrotational strain with respect to the bedding and during deformation there was no differential rotation of the local bedding and the long axis of the clasts. The fluctuation angles of the quartz clasts are much greater than 90°. This implies that the quartz clasts, and the other clasts, were originally deposited in a random fashion. The Flinn diagram shows that the pumice clasts are affected by initial compaction causing flattening in the pumice clasts that are located towards the base of the deposit. This compaction caused the pumice to have a slight initial preferred orientation parallel to the unit contacts.

The relative strains in the quartz and the pumice clast families can be attributed to differences in their viscosities. The more viscous quartz clasts are consistently less distorted than the pumice clasts. The sulphide clasts shown evidence of recrystallization while the black clasts appear to have had either a very low viscosity or have been affected by cleavage formation, or both.

The deposit is composed of clasts of massive quartz, banded quartz, phenocrystic quartz, pumice, sulphide and some unknown original material which occurs as black wisps. These clasts are within a very fine grained silicic matrix. Pillowed mafic flows occur both on top and underneath the deposit indicating deposition in a subaqueous volcanic environment. Primary charateristics such as poor sorting, normal grading of lithics, reverse to normal grading of pumice, original random orientation of clasts, and the division of the unit into massive and stratified sections imply that the deposit is a subaqeous pyroclastic flow similar to those described by Fiske and Matsuda (1964), Tasse et al (1978), and Fisher and Schmincke (1984).

REFERENCES

Bennett, G. (1978). Geology of the North East Temagami Area. Ontario Geological Survey, Report 163, 128 p.

Dunnet, D. (1969). A technique of finite strain analysis using elliptical particles. Tectonophysics, 7, 117-136.

Dunnet, D. and Siddans, A.W.B. (1971). Non-random sedimentary fabrics and their modification by strain. Tectonophysics, 12, 307-325.

Evans, B., Rowan, M. and Brace, W.F. (1980). Grain size sensitive deformation of a stretched conglomerate from Plymouth, Vermont. J. Struct. Geol., 2, 411-424.

Fisher, R.V. and Schmincke, H.U. (1984). Pyroclastic rocks. New York, Springer-Verlog, 528 p.

Fiske, R.S. and Matsuda, T. (1964). Submarine equivalents of ash flows in the Tokiwa Formation, Japan. American Journal of Science, 262, 76-106.

Flinn, D. (1956). Deformation of the Funzie Conglomerate, Fetlar, Shetland. J. Geol., 64, 480-505.

Flinn, D. (1962). On folding during three-dimensional progressive deformation. Geol. Soc. London Q.J. v118 pt4 no872, 385-433.

Friedman, G.M. (1958). Determination of size deviation from thin-section data for sedimentary petrographical studies. Jour. Geology., 66, 394-416.

Gay, N.C. (1968). Pure shear and simple shear deformation of inhomogeneous viscous fluids. Tectonophysics, 5, 211-234 and 295-302.

Hsu, M. (1971). Analysis of strain, shape and orientation of the deformed pebbles in the Seine River area, Ontario. Unpublished Ph.D. Thesis, McMaster University, 179p.

Lajoie, J., Volcaniclastic Rocks. In R.G. Walker (Ed), <u>Facies Models</u>. Geological Association of Canada. St. John's, Newfoundland. 1984.

Moorhouse, W.W. The Northeastern Portion of the Temagami Lake Area; Ont. Dept. Mines, Vol.51, Pt.6, 46p.

Ramsay, J.G. (1967). Folding and Fracturing of Rocks. McGraw-Hill, New York, N.Y., 568 p.

Tasse, N., Lajoie, J., and Dimroth, E. (1978). The anatomy and interpretation of an Archean volcaniclastic sequence, Noranda region, Quebec. Canadian Journal of Earth Sciences, 15, 874-888.

Yamada, E. (1973). Subaqueous pumice flow deposits in the Onikobe Caldera, Miyagi Prefecture, Japan. Journal of the Geological Society of Japan, 79, 535-597.